Proceedings of the Health Physics Society 2008 Professional Development School - Topics in Accelerator Health Physics (Oakland CA, January 2008)

ACCELERATOR AND BEAM PHYSICS FOR HEALTH PHYSICISTS

J. Donald Cossairt

INTRODUCTION

The acceleration and transport of particle beams constitutes a fascinating subject that merits understanding by the accelerator health physicist. The goal of this chapter is to improve knowledge and appreciation of the art of particle accelerator physics with connection to unique radiation protection concerns. It is necessary to use vector notation extensively. Vectors are printed in italic boldface (e.g., $\boldsymbol{E}$) with their corresponding magnitudes shown in italics (e.g., E). Variable names used in this chapter in general follow the custom of the published literature exemplified by the bibliography. Unfortunately, consistency of notation even within any given textbook has not been achieved. The author chose to remain close to standard notation. Much of the material covered in this chapter is found in several of the references listed. The reference citations in the text should guide the reader to particularly unique or clear descriptions. Those who specialize in accelerator design are advised to pursue formal education or detailed study elsewhere as this chapter is, by necessity, limited both in breadth and depth of material covered.

SUMMARY OF RELATIVISTIC RELATIONSHIPS INCLUDING MAXWELL'S EQUATIONS

The special theory of relativity is important at nearly all accelerators and Maxwell's equations are their basis of operation (e.g., Edwards and Syphers 1993, Wiedemann 2004). The rest energy W_O of a particle is connected to its rest mass m_O through the speed of light c (2.99792 x 10^8 m s^{-1});

$$W_O = m_O c^2 \quad (1)$$

The total energy W of a particle moving with velocity v in a given frame of reference is

$$W = mc^2 = \frac{m_O c^2}{\sqrt{1-\beta^2}} = \gamma m_O c^2 \text{, with } \gamma = \frac{W}{W_o} = \frac{1}{\sqrt{1-\beta^2}}, \quad (2)$$

where $\beta = v/c$, m is the relativistic mass, and γ is the relativistic parameter. One thus has

$$m = \frac{m_O}{\sqrt{1-\beta^2}} = \gamma m_O \quad (3)$$

Applying some algebra, the kinetic energy $T=W-W_O=(m-m_O)c^2=p^2/[(\gamma+1)m_o]$. It is clear that

$$\beta = \sqrt{1-\left(\frac{W_o}{W}\right)^2} \quad (4)$$

The momentum p of a particle in terms of its relativistic mass m and velocity v is

$$p = mv = \gamma m_o \beta c = \frac{W m_o}{m_o c^2}\left[\sqrt{1-\left(\frac{W_o}{W}\right)^2}\right] c = \frac{1}{c}\left[\sqrt{W^2 - W_o^2}\right] = \frac{1}{c}\sqrt{T(T+2W_o)}, \quad (5)$$

so that at high energies $p \approx T/c \approx W/c$ while at low energies ($T \ll W_o$) one has the familiar non-relativistic result; $p^2=(2W_o/c^2)T=2m_oT$. Another useful relation is

$$W^2 = p^2c^2 + m_o^2c^4 \quad (6)$$

It is often convenient to work in a system of units where energy is in units of eV, MeV, etc. Velocities are then expressed in units of the speed of light ($0 \le \beta \le 1$), momenta as energy divided by c (e.g., MeV c^{-1}, etc.), and masses as energy divided by c^2 (e.g., MeV c^{-2}, etc.). In these so-called "energy" units W and m are numerically equivalent. One thus avoids the use of numerical values for c or c^2. Almost universally, if a particle energy is referred to as being, say, "100 MeV", the kinetic energy T, not the total energy W, is meant.

Maxwell's equations in vacuum in SI units are needed. They connect the electric field $\boldsymbol{E}$ [Volts (V) m^{-1}]

and the magnetic field $\boldsymbol{B}$ [Tesla (T)] with the charge density $\rho(\boldsymbol{r},t)$ [Coulombs (C) m^{-3}] and current density $\boldsymbol{j}(\boldsymbol{r},t)$ [Amperes (A) m^{-2}] at a location in space $\boldsymbol{r}$ at time t. ε_o is the dielectric constant in vacuum [$10^7/(4\pi c^2)$ (C V^{-1} m^{-1}])] and μ_o is the permeability of free space [4π x 10^{-7} (V s A^{-1} m^{-1})], so $c^2=1/(\mu_o\,\varepsilon_o)$. The equations in differential (left) and integral forms (right) are

$$\nabla\bullet\boldsymbol{E}=\frac{1}{\varepsilon_o}\rho(\boldsymbol{r},t) \quad \text{or} \quad \int_{4\pi}\boldsymbol{E}\bullet d\boldsymbol{S}=\frac{1}{\varepsilon_o}\int_V\rho(\boldsymbol{r},t)dV \quad \text{(Gauss's Law),} \quad (7)$$

$$\nabla\bullet\boldsymbol{B}=0 \quad \text{or} \quad \int_{4\pi}\boldsymbol{B}\bullet d\boldsymbol{S}=0 \quad ,(8)$$

$$\nabla\times\boldsymbol{E}=-\frac{\partial\boldsymbol{B}}{\partial t} \quad \text{or} \quad \oint\boldsymbol{E}\bullet d\boldsymbol{\ell}=-\int_S\frac{\partial\boldsymbol{B}}{\partial t}\bullet d\boldsymbol{S} \quad \text{(Faraday's Law), and} \quad (9)$$

$$\nabla\times\boldsymbol{B}=\mu_o\boldsymbol{j}(\boldsymbol{r},t)+\frac{1}{c^2}\frac{\partial\boldsymbol{E}}{\partial t} \quad \text{or} \quad \oint\boldsymbol{B}\bullet d\boldsymbol{\ell}=\mu_o\int_S\boldsymbol{j}\bullet d\boldsymbol{S}+\frac{1}{c^2}\int_S\frac{\partial\boldsymbol{E}}{\partial t}\bullet d\boldsymbol{S} \quad \text{(Ampere's Law).} \quad (10)$$

The integral forms, often more useful, merit explanation. In Eq. (7) the left hand side (LHS) is the integral of electric field emerging from the closed surface that defines the volume over which the electric charge density is integrated on the right hand side (RHS). Eq. (8) reflects the nonexistence of free magnetic monopoles. In Eq. (9) the line integral of electric field around any closed integration loop (LHS) is related to the surface integral of the time rate of change of the magnetic field that flows through that loop (RHS). In Eq. (10) the line integral of magnetic field around any closed integration loop (LHS) is tied to the integrals of the current density and time rate of change of the electric field passing through the interior of that loop (RHS).

DEFLECTION OF CHARGED PARTICLES

All particle accelerators use electromagnetic forces to accelerate, deflect, and focus charged particles. The Lorentz force $\boldsymbol{F}$ [Newtons (N)] on charge q (C) with velocity $\boldsymbol{v}$ (m s^{-1}) due to applied electric field $\boldsymbol{E}$ (V m^{-1}) and magnetic field $\boldsymbol{B}$ (T) is

$$\boldsymbol{F}=q(\boldsymbol{v}\times\boldsymbol{B}+\boldsymbol{E})=\frac{d\boldsymbol{p}}{dt}, \quad (11)$$

where $\boldsymbol{p}$ is the momentum of the particle in SI units, and t is the time (s). The direction of the force due to the cross product in Eq. (11) follows the right-hand rule. Static electric fields (i.e., $d\boldsymbol{E}/dt=0$) accelerate or deccelerate charged particles while static magnetic fields ($d\boldsymbol{B}/dt=0$) can only deflect them. Nonstatic conditions couple these fields via Eqs. (9) and (10).

Nature and present-day technology have placed constraints on the design of static deflection and focusing devices. Static electric fields presently are limited a few MV m^{-1}. Currently, ferromagnetic materials are limited to about 2 T and superconductors to 4-10 T.

A common simplifying assumption is that the physical boundaries of a given deflecting or focusing element exactly define the boundary of the electric or magnetic field. For real components in an accelerator or beamline the fields extend beyond the geometrical boundaries for short distances in fringe fields. These fringe fields also deflect the particles and must be taken into account in detailed calculations since the beam elements behave as if they are a bit larger than their geometric profiles. Thus the concepts of an effective boundary and an effective field integral are used.

Before proceeding further it is necessary to mention the phenomenon of synchrotron radiation discussed elsewhere (e.g., Jackson 1999). Accelerated charged particles radiate energy, even if the acceleration is purely centripetal. Thus even particles in a circular orbit lose energy by radiating it away in the form of photons. For highly relativistic energies, a condition readily achieved for electrons, the photons emerge in a tight bundle along a tangent to any point on a circular orbit. The characteristic angle θ_c (radians) is defined to be the angle where the intensity is 1/e of that found at zero degrees and is given by

$$\theta_c=\frac{1}{\gamma}=\sqrt{1-\beta^2} \quad .(12)$$

The median energy of the power spectrum, sometimes called the characteristic energy ε_C, is given in terms of the total energy W (GeV) and bending radius R (meters) by

$$\varepsilon_c = \frac{2.218W^3}{R} \text{ (keV)}.(13)$$

For singly-charged particles of other masses m_x the characteristic energy is obtained by multiplying this result by a factor of $(m_e/m_x)^3$. The radiated power P [Watts (W)] for a circulating electron current I (mA) is

$$P = \frac{88.46W^4 I}{R}.(14)$$

For singly-charged particles of other masses m_x the radiated power is obtained by multiplying this result by a factor of $(m_e/m_x)^4$. The Large Hadron Collider (LHC) at the European Center for Nuclear Research (CERN), shortly to be operational, will be the first proton accelerator where synchrotron radiation is a phenomenon of major large-scale importance.

Deflection of Charged Particles by Static Electric Fields

A simple example of purely electrostatic deflection ($d\boldsymbol{E}/dt$=0 and $\boldsymbol{B}$=0) is illustrated in Fig. 1 where a coordinate system is defined. A "fast" particle or ion of positive charge q and momentum $\boldsymbol{p}$ that is initially following the z-axis at velocity $\boldsymbol{v}$ in vacuum encounters a pair of parallel plates of length L (m) that are biased at voltage V (V) and separated by distance δ (m). The limitation to "fast" particles is an approximation that ignores the curvature of the path followed through this beam element. A result from Eq. (7) is that between the two plates, the electric field $\boldsymbol{E}$ has a uniform value of V/δ oriented as shown. Upon entering the device, the components of the momentum are $p_z=p$ and $p_x=p_y=0$. Since $\boldsymbol{B}$=0, Eq. (11) gives

$$\frac{dp_x}{dt} = qE_x = q\frac{V}{\delta}.(15)$$

No change in p_z occurs in this system since a z-component of force is not present. Integrating over the time needed to travel through the plates and ignoring the small deviation from a straight line path for "fast" particles, an x-component p_x of momentum results at the exit;

$$p_x(\text{exit}) = q\frac{V}{\delta}\frac{L}{v} = q\frac{V}{\delta}\frac{L}{\beta c} \text{ (kg m s}^{-1}\text{)}(16a)$$

If q is, instead, taken to be in units of electronic charge, p_x is already in the convenient units of eV/c for L in meters. Expressing momentum in units of MeV c^{-1} is more useful;

$$p_x(\text{exit}) = q\frac{V}{\delta}\frac{L}{\beta}\times 10^{-6} \text{ (MeV c}^{-1}\text{)}.(16b)$$

The angular deflection $\Delta\theta$ (radians) is given exactly and in the "small angle" approximation by

$$\Delta\theta = \tan^{-1}\left[\frac{p_x}{p_z}\right] = \tan^{-1}\left[\frac{qVL}{p_z\delta\beta}\times 10^{-6}\right] = \tan^{-1}\left[\frac{qEL}{p_z\beta}\times 10^{-6}\right]; \text{ for } p_z >> p_x \ \Delta\theta \approx \frac{qEL}{p\beta}\times 10^{-6}.(17)$$

Such deflection devices are used to inject and extract beams from accelerators as inflectors (injection) and electrostatic septa (extraction). At low energies this is done using conductor planes. At high energy proton accelerators a plane of fine wires, as small as 50 μm diameter, commonly approximate one or both of the parallel plates. These devices can be tens of meters long and biased at voltages larger than 100 kV. One conductive plane is used to slice through the beam to create two beams out of one by using the electric field to give a momentum "kick" to the one part of the beam. The use of a wire plane rather than a solid plate minimizes the thickness of material struck by the beam. While the angular deflection may be small, sufficient drift space can be introduced to allow for further deflection, hence separation, by magnetic systems. The process adds a small nonzero increment to the total momentum.

Radiation Protection Considerations. The use of such devices to bend or separate particle beams has radiation safety implications. Especially for electrons, the centripetal acceleration involved in deflection can produce synchrotron radiation. Also, bending or deflection must be done correctly to assure beam delivery to the proper location such as a target or beam absorber, or some desired beam channel. Where fine-wire septa are used, the electric fields near the wires can be sufficient to produce ionization of any residual gas that might be present. These electrons can be accelerated across the gap as a so-called dark current with resultant production of x-rays.

For example, at Fermilab x-ray fields of more than 1 mGy h^{-1} have been measured near septa. Unfortunately the phenomenon is not very reproducible being dependent upon the residual gas pressure and surface conditions. The problem can be mitigated by assuring that interior surfaces are very clean, well-polished, and operated with good vacuum. Also, the small wires can become highly activated and may present problems in handling.

Accelerator physicists understandably use the small angle approximation often since deflections angles can be quite diminutive, measured in milliradians. The short-hand terms "millirads" or "mrads" can thus lead to confusion with the conventional unit of absorbed dose.

Deflection of Charged Particles by Static Magnetic fields

In a static, uniform magnetic field with no electric field ($d\boldsymbol{B}/dt=0$, $\boldsymbol{E}=0$), because of the cross product in Eq. (11), any component of $\boldsymbol{p}$ which is parallel to $\boldsymbol{B}$ will not be altered by it. Typically charged particles are deflected by dipole magnets where the magnetic field is, to high order, spatially uniform and constant or slowly-varying compared with the time the particle is present. For this situation, if there is no component of $\boldsymbol{p}$ that is parallel to $\boldsymbol{B}$ and synchrotron radiation can be ignored, the motion is circular with the magnetic force supplying the needed centripetal acceleration with the kinetic energy of the particle unchanged. The presence of a longitudinal component of $\boldsymbol{p}$ parallel to $\boldsymbol{B}$ results in a spiral trajectory with that component conserved. Fig. 2 shows the condition of circular motion. Equating the centripetal force to the magnetic force with $\boldsymbol{p}$ perpendicular to $\boldsymbol{B}$ gives

$$\frac{mv^2}{R} = qvB \text{ ,(18)}$$

where m is the relativistic mass. Solving for the radius of the circle R (meters), recognizing that $p=mv$, and changing the units of measure for momentum to MeV c^{-1};

$$R(\text{meters}) = \frac{p}{qB} \text{ (SI units)} = \frac{p}{299.79qB} \text{ (MeV c}^{-1}\text{), (19)}$$

where q in the denominator of the far right hand side is now the number of electronic charge units carried by the particle and B remains in Tesla. The product BR (T m) (or "B-rho" since "ρ" is often used to denote the bending radius) is called magnetic rigidity as it measures the "stiffness" of the particles against bending. The numerical factor in the denominator is that of the speed of light in SI units divided by 10^6.

One is often interested in the angular deflection of a magnet of length L as shown in Fig. 2. If L is only a small piece of the complete circle ($L<<R$), one can consider the circular path over such a length to be two straight line segments, one incoming and the other outgoing. The change in direction $\Delta\theta$ (deflection angle) of a particle with p (MeV c^{-1}) is given by

$$\Delta\theta = \frac{L}{R} = \frac{299.79qBL}{p} \text{ (radians),(20)}$$

where the product BL (T m) is commonly referred to as the field integral of the magnet system.

Radiation Protection Considerations. Being able to calculate the bending angle of dipole magnets can be used to deduce if the particle beam will strike some solid object near its path, a matter of practical importance. Indeed, collimation systems are designed using this formula. Bending magnets are also often placed downstream of a target to select a particular charge state, and/or momentum, of some desired secondary particle for use elsewhere by means of a collimator placed at an optimum deflection angle. Knowing the momentum of the secondary particles selected can be important in the safe design of facilities downstream.

Also, radiation safety interlocks must be designed in a way that assures that creation of correct deflection angles by the bending magnets in the system. Generally, the objective is to create so-called "fail-safe" operational conditions. If the "safe" condition requires that a given magnet be turned off, the safety interlocks are straightforward as it is relatively easy to assure that the associated power supply is "off". However, if the "safe" condition requires that a given magnet be turned "on" at a specified current, one needs to understand that large electromagnets are generally excited using circuitry that provides a constant electric current through a relatively small resistance. Short circuits can render the system unsafe if the power supply can feed the nominally correct current through the short circuit, not the magnet, without the necessary deflection of the beam. A successful solution is concurrent monitoring of the applied voltage as well as the current through the circuit; in effect monitoring the resistance of the magnet.

FOCUSING OF CHARGED PARTICLES

Some examples are given of methods for focusing charged particles. The principal technique discussed is that of quadrupoles (i.e., 4-pole magnets) operating with static, or slowly-varying (i.e. "quasi-static") electric or magnetic fields. Higher order multipoles such as sextupoles, octupoles, etc., are not considered here but are commonly used to provide special beam properties and correct for higher-order imperfections present in real components as described in the bibliography. Synopses of other methods for focusing charged particle beams are discussed here. Terminology analogous to that encountered in the study of geometrical optics of visible light is employed in charged particle optics.

Quadrupole Lenses

The Basics. Magnetic and electric quadrupoles have transverse cross sections shown in Fig. 3 along with a Cartesian coordinate system. In Fig. 3 both types are oriented to achieve the equivalent qualitative focusing effect on a particle of the same charge (+ or -). The orientations differ due to the presence of the vector cross product in Eq. (11) for the magnetic force. The polarities of the pole pieces alternate for either kind of quadrupole. The z-axis is directed along the beam and, in this case, "into the paper", the so-called optic axis of the quadrupole. Values of $y>0$ indicate upward deviations from the optic axis while values of $x>0$ measure deviations from the optic axis to "beam left", consistent with the right-hand rule. Here a simplifying assumption is that the quadrupoles (both electric and magnetic) are considered to be "thin lenses" having focal lengths much longer than their physical lengths.

Since the use of electric quadrupoles is generally limited to low energy installations while magnetic quadrupoles are used at accelerators of nearly all energies, the latter is emphasized. If the shape of the uniformly magnetized pole pieces are hyperbolae, described by $xy=\pm\frac{1}{2}a^2$, then the components of the magnetic field within the gap containing the beam are

$$B_x = -\frac{B_o}{a}\,y = -g_m y \quad (21) \qquad \text{and} \qquad B_y = -\frac{B_o}{a}\,x = -g_m x \,. \quad (22)$$

Here a is the gap radius defined in Fig. 3 and B_o (T) is the magnitude of the magnetic field strength at the pole pieces. The parameter g_m is called the gradient of the quadrupole and has units of T m^{-1}. For the electric quadrupole, the shapes of the pole pieces are given by $x^2-y^2=\pm a$, also hyperbolae. Equations analogous to Eqs (21) and (22) result with the replacement of B_o with E_o, the electric field strength at the pole pieces. $E_o=2V/a$ (V m^{-1}) connects the electric field to the applied voltage. The electric quadrupole gradient is $g_e=E_o/a$ (V m^{-2}). These are ideal quadrupoles of length L. While the ideal pole pieces are hyperbolae, cylindrical rods can be used in electric quadrupoles and semi-cylindrical pole pieces in magnetic quadrupoles to simplify manufacturing. In generalized discussions here, g is given without subscripts.

Now examine qualitatively the effect on a particle with positive charge that enters such a beam element parallel to the z-axis. If the particle trajectory is along the z-axis ($x=y=0$), then the particle will not be deflected at all since $B_x=B_y=0$ (or $E_x=E_y=0$). If the particles enter the quadrupole parallel to the optic axis but with some finite positive value of y, it will receive a deflection toward smaller values of y [see Eq. (11)]. Likewise, if it enters with a finite negative value of y, it will be deflected toward less negative values of y. Thus, a beam of such particles is said to be focused in the yz plane. However, if the particle enters with a finite positive value of x, it will be deflected toward larger x, away from the optic axis. Finally, a particle incident with a finite negative value of x will similarly be deflected away from the optic axis. Thus, a beam of such particles is defocused in the xz plane. From this qualitative discussion it is evident that more than one quadrupole is needed to achieve a net focusing effect.

Considering the situation in the yz plane, it is easy to see that the analogy with geometrical optics is instructive even in mathematical detail. One can substitute into Eq. (20) and find that the angular deflection $\Delta\theta$, assuming the validity of the "small angle" approximation, is

$$\Delta\theta = \frac{299.79 q L g_m y}{p} \text{ (radians)}, \quad (23)$$

with g_m (T m^{-1}) and y (m) inserted from Eq. (21). Likewise for the electric quadrupole based on Eq. (17) for p in MeV c^{-1} and g_e in V m^{-2};

$$\Delta\theta = \frac{q L g_e y}{p\beta}\times 10^{-6} \text{ (radians)}. \quad (24)$$

It is important that the angular deflection is proportional to the displacement from the optic axis as measured by the parameter *y*. Such linearity is a general feature of focusing phenomena.

In schematic drawings of beam elements, it is customary to show convex lenses to denote focusing elements and concave lenses to represent defocusing elements pertinent to a given plane. Bending elements are often represented by prisms. If the incident particle trajectory is parallel with the *z*-axis, the situation is shown in Fig. 4a. After deflection by a quadrupole the particle trajectory will intercept the *z*-axis at a distance *f* (m) if $\Delta\theta$ is small;

$$f = \frac{y}{\tan\Delta\theta} \approx \frac{y}{\Delta\theta} = \frac{p}{299.79qLg_m} \text{ (magnetic) or } f \approx \frac{y}{\Delta\theta} = \frac{p\beta}{qLg_e}\times 10^6 \text{ (electric).(25)}$$

This approximation is called the thin lens approximation as with visible light optics. In comparing the two versions of Eq. (25) it is observed that static electric field gradients of thousands of V m^{-2} are achievable while magnet field gradients are limited to hundreds of T m^{-1}. Notice that *f* is independent of the *y* coordinate and is called the focal length of the quadrupole. By analogy with optical thin lenses, if $f>>L$, one can write down the thin lens equation connecting the image distance z_i, with the object distance z_o;

$$\frac{1}{z_o}+\frac{1}{z_i}=\frac{1}{f} \text{ .(26)}$$

Here, $z_o>0$ and $z_i>0$ if the object is to the left of the lens and the image is to the right of the lens, forming a real image for a focusing lens with $f>0$. The situation for the defocusing plane, here the *xz* plane, is shown in Fig. 4b as a concave lens. For that plane, the equations are still valid if one applies a negative sign to the value of *f* and understands that a value of $z_i<0$ describes a virtual image. When *d* is not necessarily small compared with *f*, the phenomenon is qualitatively similar, with distances referenced to principal planes as with thick lenses used with visible light.

Quadrupole Doublets. The simplest configuration of quadrupoles is in the form of a pair of them, a quadrupole doublet exemplified in Fig. 4 for *yz* and *xz* planes. In the *yz* plane, the first is focusing with the second defocusing. In the orthogonal plane (the *xz*) the defocusing "lens" is encountered first. Commonly these elements are of similar dimensions and gradients.

Eq. (26) can now be used to explore how a quadrupole doublet can focus a parallel beam in both the *xz* and *yz* planes. For generality, the quadrupoles quad 1 and quad 2 have different focal lengths f_1 and f_2, respectively, and are separated by distance *d.* Quad 1 is focusing in the *yz* plane. For an incoming parallel beam, the object distance relative to quad 1 is $z_{yo1}\rightarrow\infty$. Thus, the image distance from quad 1 is at $z_{yi1}=f_1$. The quad 2 object distance is thus $z_{yo2}=d-f_1$. Relative to quad 2, the location of the final image will be at z_{yi2}. Employing the thin lens equation;

$$\frac{1}{z_{yi2}}=\frac{1}{-f_2}-\frac{1}{d-f_1} \text{ ,(27)}$$

where the negative coefficient of f_2 implies that lens 2 defocuses in the *yz* plane. Solving,

$$z_{yi2}=\frac{f_2(f_1-d)}{f_2-f_1+d} \text{ or } z_{yi2}=\frac{f(f-d)}{d} \text{ for identical quadrupoles .(28)}$$

Likewise for the *xz* plane the corresponding image distance z_{xi2} is

$$z_{xi2}=\frac{f_2(f_1+d)}{f_1-f_2+d} \text{ or } z_{xi2}=\frac{f(f+d)}{d} \text{ for identical quadrupoles .(29)}$$

One should notice that with identical quadrupoles,

$$z_{xi2}-z_{yi2}=2f \text{ ,(30)}$$

intuitively sensible since particles in *xz* plane are first subject to defocusing, becoming more divergent, prior to being focused. The average focal length for both planes is f^2/d.

Quadrupole Triplets. More complicated combinations of quadrupoles are employed for a variety of purposes. A particularly elegant solution to some of the limitations of quadruple doublets is the quadrupole triplet, discussed, for example, by Carey (1987). A triplet consists of three quadrupoles with the first (quad 1) and third (quad 3) of opposite polarity to the middle one (quad 2). The behavior is that of two quadrupole doublets placed back-to-back in the path of the beam. A useful special case is for quad 1 and quad 3 to have equal focal lengths *f* while quad 2 is set to have a focal length of $1/2f$ with an equal separation distance *d* between each pair. The effective focal length f^* of the system for $f>>d$ is

$$f^* = f^2\left[2d\left(1+\frac{d}{f}\right)\right]^{-1} \approx \frac{f^2}{2d} \quad .(31)$$

The symmetry and the commonly-encountered thin lens condition of $f>>d$ allows one to consider this as a single lens located at a "point" that focuses in both planes. A beam of circular cross section entrant into this system emerges with much less distortion than it would from a doublet.

Focusing Mechanisms by Dipole Magnets

Sector Magnets. Sector magnets are used to both bend and focus beams at accelerators. Fig. 5 shows both top (left) and cross-sectional (right) views of such magnets and defines a cylindrical coordinate system. The magnetic field is generalized to be non-uniform as produced by the trapezoidal pole pieces. The central ray describes the path of a particle with the specified momentum through the center of the optical system at $r=R$. Nonzero values of y measure small deviations from this pathway. The radial dependence of the vertical z-component of magnetic field B_z can be approximated by the use of a field index n defined by:

$$B_z = B_o\left(\frac{r}{R}\right)^{-n} = \frac{\text{constant}}{r^n} \text{ (32a); equivalently, } n = \frac{-dB/B}{dr/r} \text{ .(32b)}$$

n is commonly used to describe the radial dependence of the fields of many kinds of magnets.

For a uniform field magnet with $n=0$, there will be no radial component of magnetic field (i.e., $B_r=0$). However, even a uniform field wedge magnet does some geometric focusing in the horizontal plane, here along the r-axis. Qualitatively, if particles enter the magnet on paths parallel to the central ray, those with paths inside ($r<R$) the central ray will travel a shorter distance through the magnetic field than those on central ray ($r=R$) and be deflected less while those with $r\geq R$ will be deflected more. Carey (1987) has described the conditions for achieving a focus with such a system shown in Fig. 6. If $\alpha<180$ degrees (true for most practical circumstances), $\alpha+\gamma_1+\gamma_2=2\pi$ radians (180 degrees). This colinearity of the object and image points with the center of curvature of the magnet is called Barber's Rule. This approach is limited to low energies where R is not too large.

For nonzero values of n, a Taylor expansion can be used to approximate B_r;

$$B_r(z) = B_{r,0} + \frac{z}{1!}\left[\frac{\partial\, B_r(z=0)}{\partial z}\right] + \frac{z^2}{2!}\left[\frac{\partial^2 B_r(z=0)}{\partial z^2}\right] + \ldots \text{.(33)}$$

The first term and all even-order derivatives vanish from symmetry. With no currents or electric fields in the gap, the differential form of Eq. (10) can be used with Eq. (32) to obtain

$$\frac{\partial B_r(z=0)}{\partial z} = \frac{\partial B_z(z=0)}{\partial r} = -\frac{nB_o}{R}, \text{ thus(34)}$$

$$B_r \approx \frac{-nB_o z}{R} \text{.(35)}$$

The linear relationship between B_r and z creates a condition for focusing as with quadrupoles. Carey (1987) points out that only for $0<n<1$ will focusing occur in both planes simultaneously. Further, for $n=½$ one has the unique result that the focal length f in both transverse planes is the same. For a magnet with central ray of path length L referenced to the effective boundary of the magnet, a principal plane characterizing this "thick lens", the result is

$$\frac{1}{f} = \frac{1}{R\sqrt{2}}\sin\left(\frac{L}{R\sqrt{2}}\right) \text{.(36)}$$

The value of f is thus always greater than that of R and the length of such a focusing system is greater than $4R$ to accommodate the transport inside the magnet. The technique has been employed in beam lines and magnetic spectrometers at low energy accelerators. At high energies the large values of R render this approach impractical. Configurations where focusing is accomplished with $n<1$ are called weak focusing systems. At large accelerators strong focusing techniques using alternating gradient magnets having $n>>1$ with "alternating" orientations or uniform field dipoles interleaved with quadrupoles in a lattice are superior, and discussed later.

Entrance and Exit Edge Focusing by Uniform Field Dipoles. Focusing can be accomplished using the edges of fields in practical dipole magnets of uniform gap field ($n=0$) if the pole pieces are not perpendicular to the beam direction with angle ψ defined in Fig. 7. It is helpful to use coordinates s along the beam path, x transverse to

it, and z perpendicular to the bend plane (Bryant and Jenson 1993). In the horizontal (sx) plane an increase ($\psi>0$, focusing) or decrease ($\psi<0$, defocusing) of path length through the magnetic field at the entrance or exit for particles with $x>0$ occurs. For $\psi>0$ and $x>0$ the added path length $x\tan\psi$ results in an additional deflection angle α_h proportional to x, a linearity like that seen with quadrupoles;

$$\alpha_h = \frac{x\tan\psi}{R} \quad .(37)$$

Measured from the intersection of the boundary of the magnet with the central ray, a principal plane, a focal length of $R/\tan\psi$ is achieved.

The non-normal entrance of the particles also results in defocusing in the vertical (sz) plane for $\psi>0$ and focusing in that plane for $\psi<0$. Particles traveling through the magnet on or near the central ray will only be deflected vertically if they are above or below the central ray (i.e., $z>0$ or $z<0$) where they encounter a transverse horizontal component of magnetic field B_x shown in Fig. 8. Eq. (10) can determine this component as a function of z using the closed integration path shown in Fig. 8 (Side View). This integration path extends outward along the central ray beyond the fringe fields and sufficiently inward to be inside the uniform gap field B_o. With neither currents nor electric fields present inside the integration path;

$$\oint \boldsymbol{B}\bullet d\boldsymbol{\ell} = B_o z + \int_{\text{fringe}} B_s ds = 0 \quad .(38)$$

$B_o z$ is the integral along the right side of the rectangular integration path. The integral over "fringe" is the integral of component B_s along the top side of the integration path. The relevant magnetic field components along the left (where $\boldsymbol{B}=0$) and bottom (where $B_s=0$) sides are zero. However, B_s is only one component of the total horizontal component of fringe field that, due to symmetry, is perpendicular to the pole piece. The angular deflection α_v of the particles is determined by the field integral of the other component $B_x = B_s\tan\psi$ as proportional to z;

$$\alpha_v = \frac{1}{RB_o}\int_{\text{fringe}} B_x ds = \frac{\tan\psi}{RB_o}\int_{\text{fringe}} B_s ds = -\frac{\tan\psi}{R} z \quad .(39)$$

The corresponding focal length, referenced to the same principal plane as found for horizontal deflections, is ($-R/\tan\psi$). The negative sign reflects the fact that edges that focus in the xs plane ($\psi>0$) are defocusing in the xz plane, etc. Systems of such magnets can be arranged to achieve focusing in both planes as is done with quadrupoles. Obviously, both of these focal lengths become very large for values R needed at high momenta and ignore geometrical focusing.

Two special cases merit mention. If $\psi=0$, one has a uniform field sector magnet with no edge focusing. Also, at many accelerators, the magnets are rectangles, not wedges since the rectangular form is simpler to make. Rectangular magnets have no horizontal focusing since all paths parallel to the central ray go through the same field integral.

Radiation Protection Considerations Related to Beam Focusing

Some significant effects have been ignored. First, a typical particle beam will contain some spread in particle momenta. Dispersion will occur in the magnetic fields in the same way that an optical prism disperses visible "white" light into various colors. In beam designs it is common to use dispersion matching to cancel out the unwanted effects of one element by following it with another having essentially equal dispersion only in the opposite direction.

There also may be aberrations or distortions of an image such as chromatic aberration, analogous to its namesake encountered with light. For particle beams chromatic aberration is due to the momentum-dependencies of focal lengths already described. Also, no particle beam is ever perfectly parallel or exactly emergent from a geometrical point.

All particle beams possess a property called transverse emittance, discussed below and in several of the references. This quantity is expressed as the product of angular divergence and physical size; typically in units of π mm-milliradian. The explicit display of the factor π is a convenient custom. In an extracted beam the transverse emittance can generally be regarded as a constant but it can increase due to processes such as scattering from residual gas, multiple Coulomb scattering from vacuum windows, space charge effects, etc. Where the emittance is constant the product of the angular divergence of the beam envelope and its transverse size is conserved. Thus,

efforts to focus the beam tightly into a smaller spot size unavoidably result in a larger angular spread. Likewise, creation of a parallel beam results in increased size. These trade-offs must be addressed to optimize a given system with respect to beam losses on components.

The above discussion depends upon the beam axis coinciding with the optic axis of a system of one or more beam elements. Should the beam enter the system with its center off-axis, other, usually undesired, effects can result. With quadrupoles the entire beam will be deflected as if a quadrupole were a bending magnet of equivalent field integral. This effect is called steering and can produce unanticipated beam losses.

PRESENT ACCELERATOR TECHNOLOGY

Electrostatic Accelerators

Cockcroft-Walton Generators. This most elementary type of accelerator relies on elevating a terminal to high electric potential. This is done in a high voltage rectifier circuit illustrated in Fig. 9. The high voltage is achieved using rectified alternating current to charge capacitors in parallel in a so-called "ladder" arrangement applied to a load of essentially infinite resistance. The illustration shows four stages but the number is arbitrary. In this example, each capacitor thus has 1/4 V, perhaps created by a transformer, applied to it. At the terminal, a potential of V with respect to ground is achieved. The large capacitance and infinite resistance provide a stable, constant voltage. The ion source of charged particles is located inside of the terminal. Particles having charge q are accelerated by the voltage V to a kinetic energy of

$$T=qV \text{ (eV)},\quad(40)$$

with the terminal having the polarity the same as that of the chosen particles. Typically, the terminal is constructed as a metallic cube with rounded corners resting on highly resistive supports in a large, metal-lined room. The tendency toward sparking limits voltages to no more than about one MV. Such accelerators perform superbly as injectors for higher energy machines. Cockcroft-Walton generators are used only for ions, since other techniques are more efficient for electrons. Beam currents in the milliampere range are available but the energy of particles produced by a Cockcroft-Walton is not readily adjustable. Commercially available variants exist.

Van de Graaffs. Van de Graaff electrostatic accelerators are extensively used both in research in atomic, nuclear, and condensed matter physics and in more pedestrian applications. Fig. 10 shows schematically both a single stage machine and a tandem version.

Considering the single stage version first, Fig. 10 shows the arrangement for accelerating positive ions. With suitable polarity changes electrons or negative ions can also be accelerated. Electric charge is "sprayed" onto a belt that delivers it to the high voltage terminal to elevate its electric potential V. A source located in the terminal provides, in this example, positive ions of charge q for acceleration through the potential drop to a kinetic energy of $T=qV$, analysis by a momentum analyzing magnet, and then on to the intended use or next stage of acceleration. To deter sparking, the machine is enclosed in a tank filled with insulating gas, typically SF_6 at 4-6 atmospheres of pressure. V can be as large as 10 MV or more. V and hence T is very stable and can be precisely tuned. Prominent disadvantages include the large volume of SF_6, the location of the ion source in a space of finite size isolated electrically from ground, and the limited energy.

The tandem (i.e., two stage) Van de Graaff concept overcomes some of these disadvantages by placing the terminal in the middle of the tank. The charging belt (not shown) delivers positive charge to the terminal. Negative ions from an ion source, conveniently located at ground potential, or a lower acceleration stage, are accelerated in the first stage to the terminal to energy $T_1=q_1V$ where q_1 is number of electronic charges on the ions, here negative in sign. At the terminal the particles pass a stripping foil or gas where some or all of the electrons are removed and a new charge state of q_2, here positive, results. Falling through the potential V in the second stage, an additional kinetic energy of q_2V is added. The final kinetic energy available is

$$T=(q_1+q_2)V.\quad(41)$$

With this introduction to multiple charge states, terminology needs to be clarified. Accelerator physicists at ion accelerators commonly speak of beam currents in units of particle microamperes (pμA). Electrically, one electrical microampere (eμA) amounts to 6.25×10^{12} particles s^{-1} for singly-charged particles. One pμA is also associated with 6.25×10^{12} particles s^{-1} regardless of the charge state. For example, one pμA of $^6Li^{3+}$ ions is 6.25×10^{12} s^{-1}, but it only takes 2.08×10^{12} s^{-1} of these ions to result in one eμA of electric current.

Modern installations tend to use metal pellets embedded in nylon chains to replace the belts in so-called pellatrons. Providing more stable and reliable voltages, dust from the belts, a problem inside the gas vessels, is also

reduced. Terminal potentials of up to 25 MV are achieved, notably at the Holifield Radioactive Ion Beam Facility at the Oak Ridge National Laboratory (ORNL). Ions spanning the periodic table, sometimes with milliampere beam currents, are accelerated.

Radiation Protection Considerations. Due to the high potentials present, dark current sufficient to accelerate electrons and thus produce x-rays can be present in both the accelerators themselves and the ancillary components. Electrostatic accelerators are also subject to conditioning. As the accelerating voltage is gradually increased, sparking, again with the possibility of x-ray production, can occur until all surfaces are sufficiently smooth and free of defects, scratches, dust, etc. The duty factor, the fraction or percentage of time the beam is present, is an important characteristic of accelerators. Unless the ion or electron source is pulsed, Cockcroft-Waltons and Van de Graaffs typically have 100 per cent duty factors. Small duty factors can affect the response of radiation safety instruments.

Electrostatic accelerators are usually single-pass machines; the beam passes through them only one time. Therefore, to assess some radiation hazards one may need to assume that the all of the available beam can be lost at some undesired place. This can be mitigated totally or partially by successfully demonstrating that collimation or magnetic analysis in conjunction with knowledge of the beam emittance limits the amount of beam available at a critical location.

Resonant Acceleration

Electromagnetic Waves. The principal limitation of electrostatic accelerators is the constraint on beam energy due to limits in achievable values of V. Other accelerators overcome this by using time-varying electromagnetic fields to provide the acceleration. Electromagnetic waves are commonly used in ion sources as well as in the accelerators proper. Several of the references present detailed treatments derivable from Maxwell's equations [Eqs. (7)-(10)].

To simplest order electromagnetic waves are sinusoidal in functional form. For example, at a given location one can have an electric field $\boldsymbol{E}(t)$ as a function of time t;

$$\boldsymbol{E}(t) = \boldsymbol{E}_o \cos(\omega t + \xi), \text{ with } \omega = 2\pi f \quad ,(42)$$

where $\boldsymbol{E}_o$ is the amplitude, t is the time, and ξ is an arbitrary phase angle. It is common to use the angular frequency ω (radians s^{-1}) rather than radio-frequency (RF) f [cycles s^{-1}(Hz)]. The associated magnetic field $\boldsymbol{B}(t)$ has the same functional form so $\boldsymbol{E}(t)$ and $\boldsymbol{B}(t)$ satisfy Eqs. (7)-(10). The vector flow of energy in such waves in free space is the Poynting vector $\boldsymbol{S}(t)$;

$$\boldsymbol{S}(t) = \frac{1}{\mu_o}\boldsymbol{E}(t)\times\boldsymbol{B}(t) \quad .(43)$$

In vacuum the waves travel at speed of light c and are also characterized by a wavelength λ, the distance traveled between repeated points in the cycle where

$$\lambda = \frac{c}{f} = \frac{2\pi c}{\omega} \quad .(44)$$

While it would be desirable to achieve electromagnetic radiation fields where all the waves have the same wavelength, that is be absolutely monochromatic, this happens neither naturally nor artificially, even with lasers. The best attempts at generating monochromatic waves invariable result in a small spread of frequencies $\Delta\omega$ centered about the desired one ω_o. $\Delta\omega$ is typically made as small as possible due to the need for efficiency. The resultant wave pattern will tend to maintain its shape as it moves along with a velocity called the group velocity, a quantity that must be slightly less than the speed of light. But, the so-called phase velocity of the individual oscillations can exceed that of light. The product of the group and phase velocities in free space is equal to c^2. This does not violate Einstein's theory of relativity "speed limit" of c since energy or "information" moves with the group velocity.

Resonant cavities. An example of a simple cylindrical resonant cavity constructed from a highly conductive material is considered. The top frame of Fig. 11 shows such a "pill box" cavity, viewed from the side and from the end (beam's eye view). The symmetry suggests the cylindrical coordinates (r, ϕ, z) shown. The goal is to establish an accelerating electric field along the direction of the beam, along the z-axis. Consider positively charged particles entrant from the left (side view) and into the paper (right side, beam's eye view). The electric and magnetic fields inside this resonator, excited by an RF source in this so-called transverse magnetic mode (TM)

mode, have been derived (e.g., Edwards and Syphers 1993; Wangler 1998). From symmetry, the solution is independent of azimuthal angle about the z-axis and results from a boundary condition that within the cavity the component of $\boldsymbol{E}(t)$ along the z-axis must vanish at the radial boundary $r=R_c$. The solution involving the zero order Bessel function $J_o(\omega r/c)$ is

$$E_z = E_o J_o\left(\frac{\omega}{c} r\right)\cos\left(\omega t + \xi\right) .(45)$$

To satisfy the boundary condition, $J_o(\omega R_c/c)=0$. Without "crossing the Rubicon" of details of Bessel functions, this "root" of the Bessel function occurs at frequencies ω_c or f_c where

$$\omega_c = \frac{2.405c}{R_c} \text{ and } f_c = \frac{2.405c}{2\pi R_c} .(46)$$

Comparing with tabulations (e.g., Jahnke and Emde 1945), the following approximation is adequate for illustration; within 34 % for $0<\omega r/c<2.405$ and within 10 % for $0<\omega r/c<1.6$:

$$J_o\left(\frac{\omega r}{c}\right) \approx \cos\left(\frac{\omega r}{2.405c}\frac{\pi}{2}\right) = \cos\left(0.6531\frac{\omega r}{c}\right) .(47)$$

The corresponding magnetic field is an axial one with field lines shown in the right side of the top frame of Fig. 11. It is straightforward to determine the magnetic field from the electric field using Eq. 10. Application of the right hand rule shows that while the magnetic field does not serve to change the energy of the particles, it applies a focusing action upon particles with positive charge accelerated in the cavity by $E_z>0$. It is noteworthy that the resonant frequency of this particular cavity is independent of its length along the z-axis, perhaps an unfortunate result. If the resonant frequency were dependent upon the length of the cavity rather the radius, it would be easier to "tune" since its length could be readily varied (e.g., with a "piston" type of device). If, say, R_c=0.3 m then f_c=380 MHz, a value readily achieved.

Though not connected with the resonant frequency, the length L of the cavity is important. Edwards and Syphers lead us to define a transit time factor T_f as the ratio of the energy given to a particle of velocity β that crosses the cavity at peak field to the energy that would be received if the field were static at the peak value. Integrating;

$$T_f = \frac{E_o\int_o^{L/2} dz\cos\left(\frac{\omega z}{\beta c}\right)}{E_o(L/2)} = \frac{\sin\left(\frac{\omega L}{2\beta c}\right)}{\left(\frac{\omega L}{2\beta c}\right)} .(48)$$

As an example, for particles near the speed of light (β=1), T_f=0.9 implies an approximate value of L/R_c of 2/3. T_f can be used to calculate the energy gain in a given gap crossing of particle of charge q (electronic charge units) with phase angle ξ using the Panofsky equation;

$$\Delta W = qE_o\cos\xi L .(49)$$

Another consideration is the quality factor Q of resonance structures. For all resonant structures including RF circuits, Q is the ratio of the stored energy to that lost in one radian of oscillation; equivalent to the ratio of the design frequency ω_o to the frequency separation $\Delta\omega$ between the two half power points (Jackson 1999). Q quantifies the purity of the RF spectrum. Usually, the largest possible value of Q is desired to meet efficiency and "tuning" goals. For this pillbox cavity, Edwards and Syphers provide the result, with ρ_s [ohms (Ω)] as the surface resistivity (the bulk resistivity divided by the skin depth) of the cavity material;

$$Q = \frac{2.405\mu_o c}{2\rho_s\left[1+(R_c/L)\right]} .(50)$$

They observe that for typical values of ρ_s for copper of 10^{-8}-10^{-9} Ω and frequencies of about 400 MHz for this type of cavity, Q is of order 10^4. The resistivity of niobium-based superconductors is of order 10^5 smaller (Wangler 1998), with the advantage of superconducting technology clear. The term "quality factor" can be confused with that used to incorporate radiobiological effectiveness into radiation dosimetry measurements if the context is not well-understood.

It should be emphasized that pillbox cavity, in RF parlance called the TM_{010} mode, used as an example is just one of many possibilities. Some of the other possibilities are described by different values of the three

subscripts. For the pillbox cavity other resonances are possible at other values of r where $J_o(\omega_c r/c)$ is also zero. Many other configurations are used in accelerators.

The accelerating gradient (MV m^{-1}) is important. These gradients under optimum conditions are limited to about 100 MV m^{-1}. Typical operations with copper cavities at room temperature use gradients of about 20 MV m^{-1}. Lee (2004) has discussed the technical challenges. Using 40 MW of "line" power, the SLAC accelerator operates at about 20 MV m^{-1}. To achieve a gradient of 100 MV m^{-1} about 25 times more supplied power is needed (i.e., that of a large power plant). Superconducting cavities achieve such gradients using much less power.

Phase Stability. Neither "perfect" RF tunes nor single energy particles are available. One could be concerned that this fact might serve to defeat acceleration using RF techniques. Fortunately, the principle of phase stability is operative. The middle frame of Fig. 11 illustrates this qualitatively in a plot of applied electric field in an RF cavity as a function of arrival time of a particle introduced longitudinal into the cavity. The arrival time of the ideal "stable" particle is shown. It will receive an increment of energy from to the ordinate value of electric field. A particle arriving "early" either due to excessive initial kinetic energy or due to "bad timing" in previous acceleration stages will experience a lesser increment of energy and thus arrive at the next acceleration stage a bit later in RF phase. Likewise, the particle arriving "late" will receive more energy and get to the next RF cavity a bit earlier. Without performing a full quantitative treatment, it is seen that the mechanism tends to compress the kinetic energies of the ensemble of particles toward the central value, a highly desirable result.

This part of Fig. 11 also provides visualization of some other salient facets. First, it is clear that it is not desirable to time the stable particles to encounter the maximum electric field, the crest of the wave. Doing that would assure that the late particles would receive a lesser increment of energy than delivered to the stable particle with eventual loss of the late arrivals. Should the stable particle arrive after the crest of the RF wave, the early particles would likely be lost since they would achieve more than the desired energy increment. Obviously the negative excursions of the RF wave do not accelerate. In special applications they have been be used for deceleration. A qualitative picture of the phenomenon of phase stability is that of surfers on ocean waves. The skilled surfers do not ride the crest of the waves as the stable position is somewhat below it. Phase stability implies that each RF cycle creates a region in time, or equivalently in RF phase, where stable motion occurs. These regions are called buckets some or all of which may be populated with beam particles. The group of beam particles in a particular bucket is called a bunch. A refinement of the phase stability concept will be discussed later.

Linear Accelerators

Drift Tube Linacs. The bottom frame of Fig. 11 shows conceptually a modern drift tube linear accelerator or "linac" (DTL) of the Alvarez type. These accelerators are most useful for protons and heavier ions, with serious limitations pertaining to electrons shortly to be discussed. In the linac segment shown, a beam already accelerated by a lower energy stage enters from the left. This type of DTL works best in the approximate domain $0.04<\beta<0.4$. RF energy feeds the entire enclosure, called a tank, that itself is a resonant structure typically containing a few tens of individual drift tubes. The beam is exposed to electromagnetic fields only in the gaps since each conductive drift tube provides a Faraday cage shielding the moving particles from the RF fields while they are "drifting" through it. No acceleration of the particles occurs during the time spent inside the tubes. Each short gap acts as a resonant cavity and at each gap crossing the particles receive an increment of kinetic energy. This works if the drift tube lengths D are designed in a full wave mode so that at each point

$$D = \beta\lambda, \quad (51)$$

where λ is the RF resonant wavelength and βc is the particle velocity through that particular drift tube. Since the RF fields in all the gaps are synchronized and λ/c is the time duration of one RF cycle, it is clear that a particle traveling through a given drift tube will, ideally, upon emerging from it encounter the electromagnetic field exactly at the same phase as it did in the previous gap and thus continue being accelerated. Obviously for non-relativistic particles, the first drift tubes encountered are shorter than those encountered with increased velocity. Quadrupole magnets can be incorporated in selected tubes to provide transverse focusing of the particles.

Other types of DTLs are possible, notably the Wideröe design, where half-wave drift tubes are interleaved with alternating polarities of the RF fields in the gaps. These were used historically but the RF structures were found to have lower values of Q than the Alvarez design. These and other considerations rendered the Alvarez type preeminent. However, the Wideröe DTL is rather good for low velocity ions (e.g., $\beta<0.03$) and low frequencies (e.g., $f<100$ MHz).

While DTLs are quite effective in delivering high (mA) beam currents there are notable limitations as

discussed by Wangler (1998). One is that the part of the length of the machine devoted to the drift tubes contributes no acceleration. Another is that the first drift tubes are generally too short to accommodate focusing quadrupoles. Also, by its nature as a resonant structure continuous variability of beam energies is unavailable. Care is needed to assure that peak surface electric and magnetic fields are kept within technological limits to avoid both sparking and excessive heating. Heating from the large amount of applied electrical energy is an especially important consideration since it can result in changes in the physical dimensions of the RF structure and thus the resonant frequency. Well-regulated cooling systems are crucial. Due to the pulsed beam structure and ignoring RF microstructure, typical duty factors of DTLs are only a few per cent or so.

Resonant acceleration always results in a pulsed beam. Provisions are commonly made prior to injection into the linac to create a pulsed beam of the desired frequency at low energies. While RF acceleration guarantees that a pulsed beam will be produced, without pulsing the injected beam, the portions of the beam that fail to be accelerated would be lost in the linac itself, a potential source of unwanted beam heating and undesirable radioactivation.

Coupled-Cavity Linacs. At higher velocities the DTL is rather inefficient and becomes lengthy. As $\beta \rightarrow 1$ one no longer needs to be concerned with changes in β as acceleration proceeds, so that coupled-cavity structures become efficient (Wangler 1998). The "coupling" refers to how the cavities are connected one to another to maintain synchronization. In the common side-coupled version, the cavities are excited electromagnetically along their sides, usually alternating from one side to the other to maintain symmetry. Other methods of coupling are done, such as along the beam axis where a linear array of resonant cavities are placed in line continuously to form a multi-cavity acceleration structure. The individual cavities operate in a TM_{010} standing wave; that is, "stationary" mode. This type of structure provides two acceleration gaps per $\beta\lambda$ and are effective in the velocity range $0.4<\beta<1$. They are used for both electrons and heavy particles. For electron colliders, the standing wave design is especially useful since such standing waves represent a superposition of two synchronous traveling waves from opposite directions, each capable of accelerating a beam of particles. Given the short wavelengths at high frequencies, mechanical tolerances can be important. Fine tuning is often done by applying mechanical adjustments such as microscopic deformations along with electromagnetic "tweaking" using, for example, ferrite tuners.

Electron Linacs. Electrons present a unique situation even at low energies. An electron with a kinetic energy of T=3 MeV has β=0.989. A continuous, uniform wave guide is a tempting concept for an accelerator. But the phase velocity in such a structure always exceeds the speed of light, preventing synchronization with the beam particles since the form of the wave would race ahead of the particles being accelerated. Also, a longitudinal component of electric field is necessary to provide the accelerating force. The solution is to break up the wave guide into periodic structures that act as individual resonance cavities. This limits the bandwidth by suppressing wavelengths that do not "fit" and has been accomplished by installing "loading" disks, with a hole for the beam to pass through, perpendicular to the beam direction. The effect is to create a longitudinal series of *de facto* short cavities that have the required longitudinal component of electric field. The electrical resistance of the load serves to reduce the phase velocity to below the speed of light. This is called a disk-loaded or iris-loaded waveguide.

High RF frequencies up to tens of GHz (e.g., 3 GHz at SLAC) are used in high energy electron linacs. Improved duty factors approaching continuous wave (CW) conditions are possible (Wangler 1998).

Recirculating linacs line up sets of linacs to achieve desired energies in steps, with intervening circular arcs to direct the beam from one linac stage to the next. This approach has generally been limited to electrons. The Continuous Electron Beam Accelerator Facility (CEBAF) accelerator at the Thomas Jefferson National Accelerator Facility (TJNAF) is the most prominent recirculating linac and also provides continuous wave operation.

Radio-frequency Quadrupoles. Radio-frequency quadrupoles (RFQs) operable in the velocity range of $0.01<\beta<0.06$ combine the focusing capabilities of electric quadrupoles with the acceleration by RF fields. They can be considered to be a type of linac. RFQs are used only for protons and ions because electron guns can more readily supply electrons of higher velocities.

The discussion of Wangler (1998) is particularly helpful. Fig. 12 shows an end ("beam's eye") view along with a side view of a RFQ. The device is a RF cavity where four "vanes" are excited by an applied RF field with the time dependence described by Eq. (42). By comparison with Fig. 3 one notices the electric quadrupole configuration of the vanes and similar polarity arrangement, but with "modulation" as a function of z, also shown in the side view. At any given instant the beam particle will experience a focusing or defocusing action dependent upon its transverse location in the xy plane and coordinate z. The ratio of the largest gap radius to the smallest gap radius is the modulation parameter m. Fig. 12 also defines the unit cell length $L=\beta\lambda/2$, where λ is the RF wavelength. The two vanes aligned with the yz plane (vertical in Fig. 12) are modulated out of phase with the two

vanes aligned with the *xz* plane.

There are two reasons for the modulation. First, the electric field will in general be oriented "normal" (i.e., perpendicular) to the conductive material of the vanes and thus, due to the modulation, can have the longitudinal component necessary for acceleration when the phase with the beam is "right" for beam particles at off-axis locations. Second, with unmodulated vanes, from symmetry there would be no electric field on the axis at all and hence no longitudinal component that could provide an accelerating force to beam particles aligned "on axis", the desired location for the beam. Modulating the vanes creates the desired longitudinally alternating RF electric field. The shape of the modulations creates conditions where the particles stay synchronized with the accelerating part of the cycle while proceeding down the RFQ since the travel through each modulation cycle takes the same amount of time. Phase stability applies to particles that are slightly "early" or "late". Alternating the modulations of the vertical and horizontal vanes through each repetition of the cell structure also alternates the strength and sign of the instantaneous quadrupole focusing gradients just as it would in a long sequence of static electric quadrupoles of alternating polarity.

In a manner conceptually similar to that done for DTLs for synchronous particles (i.e., those that are "on time"), the energy gain per cell ΔW, the spatial average of the peak axial accelerating field over the RFQ unit cell E_o, and transit time factor T_f, all as functions of radial coordinate r in the cell and particle phase ξ, are calculated by Wangler (1998). To properly take into account the usual sinusoidal shape of the modulations, only the results of the complex calculation are given;

$$\Delta W = \frac{q\pi A V_o I_o(kr)\cos\xi}{4}, E_o = \frac{1}{L}\int_o^L E_z dz = \frac{2AV_o}{\beta\lambda}, \text{ and } T_f = \frac{\int_o^L E_z \sin kz dz}{\int_o^L E_z dz} = \frac{\pi}{4}. \quad (52)$$

Here $k=1/\lambda$ and is called the wave number and A is the accelerating efficiency, a parameter dependent upon the value of m [e.g. $A=0$ for no modulation ($m=1$)]. V_o (V) is the applied potential and the integrals are over the unit cell length $L=\beta\lambda/2$. The product AV_o is the effective axial voltage applied over the length of the unit cell while E_o is the average axial electric field. $I_o(kr)$ is the modified Bessel function of the first kind of zero order. $I_o(kr)$ is monotonically increasing and slowly varying for practical values of kr and is well-approximated by

$$I_o(kr) \approx 1 + \frac{(kr)^2}{4}. \quad (53)$$

Assembling all of this, one finds that

$$\Delta W = qE_o T_f I_o(kr) L\cos\xi. \quad (54)$$

From the functional form, it is obvious that off-axis synchronous particles receive more energy gain than do those aligned with the optic axis (i.e., the z-axis). However phase stability conditions apply and this generally gets self-corrected at subsequent cells.

A pulsed beam results from the operation of a RFQ. RFQs are generally designed to produce a specific energy for a particular particle type since the cell lengths are not adjustable. Series of RFQs have been used and superconducting versions exist. In the transverse plane the ideal vane shapes are hyperbolae, but RFQs have successfully used conductive rods of circular cross sections with the diameter of the rods made large compared with the modulated aperture. The modulated shape can be difficult to construct. Practical RFQs have been successfully made using conductive rods turned on a lathe to create longitudinal trapezoidal profiles.

Compared with Cockcroft-Waltons and Van de Graaffs, RFQs can provide high intensity beams with a more compact infrastructure. By using the electric quadrupole focusing technique, they also take advantage of the fact that for low velocity particles, practical electric field focusing forces are stronger than are corresponding magnetic focusing forces at low velocities, reflective of the velocity factor in Eq. (11). RFQs are used as injector accelerators at many installations. At some installations, RFQs with variant vane or rod structures are used to contain and store, rather than to accelerate, ion beams.

Radiation Protection Considerations. All linear accelerators involve the use of radio-frequency devices of considerable energy. Aside from notable electrical hazards, the high power radio tubes used to generate the RF fields can produce dark currents with x-ray production. Also, for convenience of operation, major RF components are located external to the accelerator enclosures to facilitate tuning, status monitoring, repair, and replacement without undue disruption to operations. Therefore, x-ray hazards may exist in locations accessible to personnel with the need for radiation field characterization and monitoring, the application of radiation shielding, and personnel

radiation dosimetry.

A condition known by RF engineers as multipacting can be important (Livingood 1961; Wangler 1998). This is a resonant condition that can repeatedly accelerate electrons across a gap, then drive them back to a surface where they liberate more electrons, then accelerate the additional electrons and repeat the cycle thus creating an avalanche of electrons. Likewise, electron field emission can result from strong surface electric fields with production of x-rays and generation of heat. These processes are undesirable both from the radiation protection standpoint and as loss of useful power into heat. They also add electrical impedance and thus reduce the quality Q of the RF resonance.

Linacs are "single pass" machines so one must consider the possibility that the entire beam current may be delivered to some undesirable location. The duration of this loss of beam may be limited by other considerations that need proper assessment.

When conducting radiation surveys or operating radiation monitoring near an operating resonant accelerator, especially in the vicinity of the RF equipment, assurance is needed that the survey instrument is sufficiently insensitive to the RF. The use of Faraday shields of conductive material around a radiation detector may, with proper testing and verification, be a remedy.

Cyclotrons, Synchrocyclotrons, and Betatrons

Cyclotrons. While linear accelerators serve major roles in industry, medicine, and research, their most serious limitation is their length along with the usage of entire RF resonant structure only once during the acceleration cycle. For low energy protons and positive ions where relativistic concerns do not dominate and synchrotron radiation is negligible, the cyclotron is a proven solution. The top frame of Fig. 13 shows a plan view of a typical cyclotron located in the gap of a large electromagnet that supplies a uniform magnetic field, here directed into the paper, along the z-axis. Ions are injected into the machine at the center or at a small value of the radius r. Historic machines used internal ions sources producing particles having very small initial kinetic energies. Modern installations use energetic ions produced by external ion sources or lower energy injector accelerators. The structure shown is set up to deflect positively charged particles along the indicated circular path. Within the magnet gap, one finds a pair of hollow D-shaped conductors, naturally called "dees". RF supplied across the dees creates an accelerating electric field along the particle trajectories for particles that pass across the gap at the "right" time. It is common for one dee to be replaced by an electrically conductive planar structure called a dummy dee, using electromagnetic "reflections" to avoid keeping two large resonant structures identical. Especially with external ion sources, electrostatic deflectors called inflectors are used to direct the beam into the first (innermost) orbit. Extraction is commonly accomplished using electrostatic septa, typically with solid electrodes rather than fine wires.

This discussion generally follows that of Lee (2004). When the particles are not crossing one of the two gaps, they are within the conductor of a dee and hence shielded from the RF while still subject to deflection by the static magnetic field. From Eq. (18), the velocity v of the particle at radius r deflected by magnetic field B_o is

$$v = \frac{qB_o r}{\gamma m_o} . \quad (55)$$

In Eq. (55) the relativistic parameter γ is explicitly shown for reasons that will shortly be clear. Taking the path as circular, one orbit time is $2\pi r/v$ and the orbit frequency is $v/2\pi r$ (Hz). This leads to the synchrotron (angular) frequency ω_{syn};

$$\omega_{syn} = 2\pi \frac{qB_o}{2\pi\gamma m_o} = \frac{qB_o}{\gamma m_o} . \quad (56)$$

For non-relativistic particles, one has the similar cyclotron frequency, ω_{cyc};

$$\omega_{cyc} = \frac{qB_o}{m_o}, \text{ for } \gamma \approx 1. \quad (57)$$

The lack of dependence of this orbit frequency on r at low energies is important as it allows the orbits to be isochronous for constant magnetic field strength B_o. To provide acceleration, the RF frequency must be an integer multiple h of ω_{cyc} called the harmonic number;

$$\omega_{RF} = h\omega_{cyc} \quad (58)$$

To assure that when the particle arrives at the next gap between the dees, the accelerating electric field must be of opposite sign and hence appropriately oriented for further acceleration. The detailed design places constraints on h. For example in the "classic" cyclotron with two gaps 2π radians apart in the orbit, h must be an odd number to accomplish acceleration.

As a result of acceleration, γ increases above unity. To maintain continuous operation, one cannot simply reduce the applied RF frequency along with γ as implied by Eq. (56) to keep the highest energy particles synchronous for that would cause the lower energy particles simultaneously being accelerated to fall out of phase with the RF in the gaps. Using Eqs. (5), (18), and (56), and, for now, staying with SI units, one finds

$$r = \frac{p}{\omega_{syn}\gamma m_o} = \frac{\gamma}{\omega_{syn}\gamma m_o}\frac{W_o}{c}\left[1-\left(\frac{W_o}{W(r)}\right)^2\right]^{1/2} = \frac{\gamma m_o c^2}{\omega_{syn}\gamma m_o c}\left[1-\left(\frac{W_o}{W(r)}\right)^2\right]^{1/2}$$
$$= \frac{c}{\omega_{syn}}\left[1-\left(\frac{W_o}{W(r)}\right)^2\right]^{1/2} \quad .(59)$$

To achieve the much-desired spatially constant RF frequency, from Eq. (56) the magnetic field component B_z must be scaled with r by first solving Eq. (59) for total energy $W(r)$;

$$W(r) = W_o\left[1-\left(\frac{\omega_{syn}^2 r^2}{c^2}\right)\right]^{-1/2}, \text{ then } (60)$$

$$B_z = \frac{\omega_{syn}\gamma m_o}{q} = \frac{\omega_{syn}W(r)}{qc^2} = \frac{\omega_{syn}}{qc^2}W_o\left[1-\left(\frac{\omega_{syn}^2 r^2}{c^2}\right)\right]^{-1/2} = \frac{\omega_{syn}}{q}m_o\left[1-\left(\frac{\omega_{syn}^2 r^2}{c^2}\right)\right]^{-1/2} \quad .(61)$$

At cyclotrons, it is useful to express particle or ion rest masses in units of the atomic mass unit m_u (1.0 m_u = 931.494 MeV c^{-2} = 1.66054x10^{-27} kg) and beam charge in units of electronic charge. Making this conversion with the help of Eq. (19);

$$B_z = \frac{\omega_{syn}}{q}\frac{931.49}{299.79}A\left[1-\left(\frac{\omega_{syn}^2 r^2}{c^2}\right)\right]^{-1/2} = 3.107\frac{\omega_{syn}}{q}A\left[1-\left(\frac{\omega_{syn}^2 r^2}{c^2}\right)\right]^{-1/2} \quad ,(62)$$

where the atomic mass A (atomic mass units, amu) is the particle atomic mass and B_z is in Tesla.

The traditional method for accomplishing this is to install trim coils in the magnet gap to provide a means of gradually increasing the applied magnetic field with radius r so that the magnetic field increases as a function of r along with γ. The trim coils are generally provided as a set of multiple elements to provide flexibility of operation for a variety of ion masses and charge states. Altering the final energy or charge state of a cyclotron typically takes a finite amount of time to execute a number of small adjustments to achieve stable acceleration because of the need to adjust the trim coil currents along with the RF frequency.

The result is an isochronous cyclotron. The magnetic field now has a field index $n<0$, implying a radial component of magnetic field B_r that increases as a function of r. The orbits are thus unstable vertically (i.e., along the z-axis). This unacceptable condition is addressed by creating "hills" and "valleys" in the magnetic field using regions of elevated and reduced magnetic field strength as shown in the bottom frame of Fig. 13. To the left is shown an example using sector focusing. The sector magnets can focus vertically because they are not truly uniform due to the additional field of the trim coils and, also, the beam particles have a slight non-perpendicular entrance into their fringe fields. Completely separate sector magnets are successfully used in cyclotrons, exemplified by the superb 200 MeV machine at the Indiana University Cyclotron Facility (IUCF). Spiral-ridge designs are also used to introduce vertical focusing by having the particles encounter wedge fields at non-normal incidence. The spirals provide increased entry angles ψ at the larger values of r [see Eqs. (37) and (39)]. Either method results in manageable oscillatory phenomena along both the vertical and radial axes. Both types represent azimuthal varying field (AVF) cyclotrons, a term synonymous with isochronous cyclotron. The flutter amplitude F_l measures the differences between the peak magnetic field in the hills B_h and lowest magnetic field in valleys B_v related to the average during the orbit B_{av};

$$F_l = \frac{B_h - B_v}{2B_{ave}} .(63)$$

For extracted particles at radius R, one has momentum $p(R)=\gamma m_o \beta c$ and kinetic energy

$$T(R) = m_o c^2 (\gamma - 1) = \frac{p^2(R)}{(\gamma+1) m_o} (64)$$

at radius R. For ions of atomic mass number A, the ratio of kinetic energy to atomic mass number $K=T(R)/A$ in terms of the magnetic rigidity B_oR (T m) is found to be useful;

$$K = \frac{T(R)}{A} = \frac{q^2 \gamma^2 B_o^2 R^2}{(\gamma+1) m_o} \text{ (SI units)} = \frac{96.48 \gamma^2 (B_o R)^2}{(\gamma+1)} \frac{q^2}{A} \left(\frac{\text{MeV}}{\text{amu}} \right) (65)$$

where on the far right q is the net charge carried by the ion in units of electron charge.

Considering the radial spacing between the orbits, if RF across the accelerating gaps results in a voltage drop of V_o (MV) per orbit, a kinetic energy of $T_N=qNV_o$ (MeV) results after N turns. Solving Eq. (18) for r_N (m) and converting units, a dependence on $N^{1/2}$ is found;

$$r_N = \frac{p_N}{qB} = \frac{\left[(\gamma+1) m_o A q N V_o \right]^{1/2}}{qB} = \frac{\sqrt{931.49} \left[(\gamma+1) A q N V_o \right]^{1/2}}{299.79 qB} = \frac{0.1018}{B} \left(\frac{(\gamma+1) A V_o}{q} \right)^{1/2} N^{1/2}, \quad (66)$$

with q in units of electron charge and A in amu. After many orbits the spacing can be quite small, so extraction septa needing careful design to reduce the amount of "stray" beam intercepted.

Synchrocyclotrons. Instead of increasing the magnetic field with radius as in cyclotrons, an alternative is to modulate the RF frequency according to Eq. (56) to maintain a constant orbit frequency. This is done in synchrocyclotrons. Proton energies up to about 1.0 GeV can be obtained but the beam is a pulsed one since only one group of particles can be accelerated at a time. Thus, in contrast with the high duty factor of cyclotrons, synchrotons generally have a low duty factor. Due to practicalities of magnet power supplies, the cycle times generally are related to the line power frequency (i.e., 60 Hz in the U.S. or submultiples). They largely have been superseded by modern cyclotrons (at lower energies) and synchrotrons (at higher energies.)

Betatrons. With the strong dependence on γ, the cyclotron concept is inappropriate for electrons. A historic, but instructive, solution to this problem is the betatron. Though superseded by linacs and synchrotrons as the vehicle of choice for accelerating electrons, betatrons illustrate important features of other circular accelerators. Fig. 14 shows a side view of a betatron (top) along with a useful coordinate system (bottom). The betatron is unique in using electromagnetic induction to provide the electric field. Low energy electrons are introduced into the magnetic field of the betatron at radius R with a low magnetic "guide" field present. The magnetic field is smoothly increased to effect the acceleration. Repeating Eq. (9);

$$\oint \boldsymbol{E} \cdot d\boldsymbol{\ell} = -\int_S \frac{d\boldsymbol{B}}{dt} \cdot d\boldsymbol{S} .(67)$$

This equation relates the induced electric field $\boldsymbol{E}$ around the orbit to the rate of change of the integral of magnetic flux enclosed by the orbit. From symmetry, if the magnetic field is increasing at rate $d\boldsymbol{B}/dt$ (not necessarily a constant), the corresponding electric field $\boldsymbol{E}$ along the path of the orbit is uniform and independent of θ. Eq. (67) amounts to

$$2\pi R E(R) = \pi R^2 \frac{dB_{ave}}{dt} .(68)$$

Thus the electric field is given by

$$E(R) = \frac{1}{2} \frac{dB_{ave}}{dt} R .(69)$$

From Eq. (11), the equation of motion is straightforward;

$$\frac{dp}{dt} = \frac{1}{2} qR \frac{dB_{ave}}{dt} ,(70)$$

Defining the guide field B_g at the orbit to be half of the average field enclosed by the orbit B_{ave} one has the betatron condition for both SI and "energy" units (q=1 for electrons) and B_gR (T m);

$$p = qB_gR \text{ (SI units)} = 299.79 B_gR \text{ (MeV c}^{-1}\text{)} .(71)$$

This accelerates the electrons in an orbit of constant radius. Betatrons are also ramped at frequencies connected with the line power frequency (60 Hz in the U. S.) The vacuum chamber of a betatron cannot be a continuous conductor because during operation the changing magnetic field would generate a current in that conductor, as in a transformer, and not accelerate the beam.

The transverse stability of this situation is instructive especially when extended to other circular accelerators. Since the betatron condition imposes a field at the orbit of less strength than that at the gap, the field index n>0 has plausible focusing properties. From symmetry the magnetic field has two components B_z and B_r, with no component of $\boldsymbol{B}$ along the orbit. The equation of motion of particles near the orbit is the magnetic term of Eq. (11). Since $p=mv$, in cylindrical coordinates (r,θ,z) (Edwards and Syphers 1994; Livingood 1961);

$$\frac{d^2\boldsymbol{r}}{dt^2} = \left[\frac{d^2r}{dt} - r\left(\frac{d\theta}{dt}\right)^2 \right] \hat{\boldsymbol{r}} + \frac{d^2z}{dt^2}\hat{\boldsymbol{z}} = -q\frac{vB_z}{m}\hat{\boldsymbol{r}} - q\frac{vB_r}{m}\hat{\boldsymbol{z}} .(72)$$

The components along the θ-axis are zero. The second term in the coefficient of the radial unit vector leads to centripetal acceleration. Simplifications arise from taking the angular frequency of the orbit to be constant for small deviations from the equilibrium orbit R and $\omega=d\theta/dt=v/R=qB/m$. Equating the axial ($z$-axis) components and taking B_r from Eq. (35);

$$\frac{d^2z}{dt^2} = -\frac{qB_g}{m}\frac{v}{R}nz = -\omega^2 nz . \quad (73)$$

The solution is the equation of a harmonic oscillator, the mathematical description of a steel spring. The frequency is $\omega n^{1/2}$ and the amplitude is z_{max} with arbitrary phase angle ϕ;

$$z(t) = z_{\max}\cos\left[\left(\omega\sqrt{n}\right)t + \phi\right] .(74)$$

Radially, small deviations from the equilibrium orbit $r=R+\zeta$ are considered (Livingood 1961);

$$\left[\frac{d^2r}{dt} - r\left(\frac{d\theta}{dt}\right)^2\right] = \left[\frac{d^2r}{dt} - \frac{v^2}{r}\right] = -q\frac{v}{m}B_z(r) ,(75) \text{ then}$$

$$\frac{d^2\zeta}{dt^2} - \frac{v^2}{R+\zeta} = -qvB_z(R+\zeta) .(76)$$

In the chosen approximation for small ζ;

$$\frac{1}{R+\zeta} = \frac{1}{R}\left(1+\frac{\zeta}{R}\right)^{-1} \approx \frac{1}{R}\left(1-\frac{\zeta}{R}\right) (77) \text{and}$$

$$\frac{d^2\zeta}{dt^2} - \frac{v^2}{R}\left(1-\frac{\zeta}{R}\right) = -\frac{qv}{m}B_z(\zeta) .(78)$$

Recognizing from Eq. (18) that $v^2/R=qvB_g/m$ and rearranging;

$$\frac{d^2\zeta}{dt^2} + \left[B_z(\zeta) - B_g\right]\frac{qv}{m} + \frac{qvB_g}{m}\frac{\zeta}{R} = 0 .(79)$$

But with a Taylor expansion, $B_z=B_g+\zeta dB/dr+\ldots$, one can approximate B_z-B_g with $\zeta dB/dr$. Doing this, making other substitutions $v=\omega R$ and $q/m=\omega/B_g$, and recognizing that $n=-RdB/(B_gdr)$;

$$\frac{d^2\zeta}{dt^2} + \frac{R}{B_g}\frac{dB}{dr}\omega^2\zeta + \omega^2\zeta = 0 \rightarrow \frac{d^2\zeta}{dt^2} + \omega^2(1-n)\zeta = 0 .(80)$$

Like for Eq. (73), the solution of Eq.(80) is a harmonic oscillator of frequency $\omega(1-n)^{1/2}$ and amplitude ζ_{max};

$$\zeta(t) = \zeta_{\max} \cos\left[\left(\omega\sqrt{1-n}\right)t + \phi\right] . (81)$$

The axial and radial oscillations, representative of those of other circular accelerators, are called axial and radial betatron oscillations. The numbers of betatron oscillations per orbit axially [$\nu_z = n^{1/2}$] and radially [$\nu_r = (1-n)^{1/2}$], not integers, are called the tune. In the betatron the orbits are unstable if the condition $0<n<1$ is not satisfied. At the extrema of this domain there are no oscillations in one of the coordinates resulting in an unstable "drift". For $n>1$ the argument of the radial oscillations becomes an imaginary number, describing an absorption process rather than oscillation. As seen with the cyclotron, the $n<0$ situation is radially defocusing. When $n=1/2$ the tunes in both dimensions are the same, explaining the unique focal properties of the $n=1/2$ magnet. Eqs (73) and (80) are called the Kerst-Serber equations and when generalized apply to axial and radial motions in all weak-focusing circular accelerators. The duty factor limitations experienced at synchrocyclotrons are applicable to betatrons.

Radiation Protection Considerations of Cyclotrons, Synchrocyclotrons, and Betatrons. RF sources and deflection devices such as inflectors and electrostatic septa can produce *x*-rays. Furthermore, external ion sources and especially lower energy injector accelerators can produce activation upon injection into the higher energy stage if the beam emittance is not matched to that accepted (i.e., the acceptance) by the higher energy stage. Orbits have to be tuned carefully upon injection and extraction to minimize radioactivation of components. Especially at betatrons, synchrotron radiation with consequent x-ray production arises as a consideration. The loss of electrons can produce photons and photoneutrons copiously. The massive magnets of these machines can present radioactive material handling problems at the time of decommissioning. Likewise any large copper components can be the locus of long-lived radioactivation.

Synchrotrons

Strong-Focusing Synchrotrons. The ultimate circular accelerator at present is the strong-focusing synchrotron, simplistically describable as a combination of the favorable characteristics of the linac, betatron, and synchrocyclotron. In the betatron, while the region interior to the orbit is necessary to generate the electric field by induction, it serves no other purpose. Likewise, the requirement of a large magnet is the chief limitation of the synchrocyclotron. Instead of magnetic induction, RF energy is used to accelerate particles traveling in an orbit of constant radius R without needing a magnetic field inside of the large orbit in a synchrotron. Here a pulsed beam with a desirable time structure is accelerated up to some energy corresponding to an orbit of radius R by an injector accelerator and inserted into a ring of magnets set to achieve a circular orbit at the injection momentum. The injection energy should be sufficiently high to assure achievement of a reproducible magnetic field $\boldsymbol{B}$ of sufficient quality to be free of "low field" effects (e.g., eddy currents, hysteresis effects, power supply instabilities). The particles are then accelerated in the ring guided by magnetic field $\boldsymbol{B}$. In the ring, the particles pass through one or more gaps supplied with RF energy (as in the linac, cyclotron, or synchrocyclotron) and gain increments of energy that are synchronously (hence the the name of the accelerator) matched to a gradual ramping (increase) of $\boldsymbol{B}$ to maintain constant orbit radius R. The cycle time of ramping is slow enough so that in the synchrotron the acceleration provided by the $d\boldsymbol{B}/dt$ term in Eq. (9), the operating principle of the betatron, is unimportant compared with that provided by the RF.

Cyclotrons, synchrocyclotrons, and betatrons are all weak-focusing devices, with focal lengths scaled to radius R. At the large values of R needed at high momenta such accelerators are impractical since apertures become huge in order to accommodate the necessary focusing of beams of correspondingly large transverse dimensions. For example, the now-dismantled 6 GeV Bevatron at the Lawrence Radiation Laboratory (LRL, now LBNL) had a field index $n=0.6$ with an aperture of 1.16 m (vertical) by 0.30 m (horizontal) (Livingood 1961)!

The strong-focusing synchrotron is the solution and is described in great detail in several of the references with only vignettes of some of the salient features provided here. Many important effects are relegated to the bibliography. Alternating-gradient magnets like that illustrated in Fig. 5 can be reversed in the "sense" of their radial deflections around the ring to achieve the necessary stability of focusing. Very "strong" focusing, indeed, is used. For example in the 30 GeV Alternating Gradient Synchrotron (AGS) at Brookhaven National Laboratory (BNL) $n=357$ (Livingood 1961). Such magnets with their complicated pole-piece shapes are expensive to manufacture on a large scale so an alternative is needed.

Separated function strong-focusing synchrotrons are the current state-of-the-art for large machines. The discussion here generally, but not exclusively, follows that of Edwards and Syphers (1993). Some features of a particularly useful summary by Desler and Edwards (2004) are also employed. The top frame of Fig. 15 is a sketch

of such an accelerator. Uniform field dipoles supply the bending field while quadrupoles of alternating focusing sense are interspersed, commonly equally spaced, around the ring in a focusing-defocusing FODO lattice. Each "dipole" or "quadrupole" could be a series or string of individual, identical magnets. Fig. 15 shows two straight sections, one with the RF cavities and the other used for some other purpose such as injection, extraction, or an experiment. Multiple straight sections for all of these purposes are feasible and are used. At machines with large R, the dipole magnets are longitudinally rectangular. In the remainder of this chapter examples of key parameters found in Fermilab synchrotrons are provided (Edwards and Syphers 1993; FMI Website 2007).

Phase Stability and Transition Crossing. An "ideal" particle on the reference orbit will pass between any two points of reference such as complete orbits, in a time interval $\tau=L/v$ where L is the path length and v is the speed of travel along the orbit. If the ideal path is not followed with deviations in the path length ΔL or the speed Δv, the fractional change in τ is

$$\frac{\Delta\tau}{\tau}=\frac{\Delta L}{L}-\frac{\Delta v}{v}. \quad (82)$$

Intuitively, τ increases with longer path length and decreases with increased speed. The fractional change in path length $\Delta L/L$ between two reference locations, typically but not exclusively an entire orbit, is generally proportional to the fractional change in particle momentum $\Delta p/p$ through a dispersion coefficient dependent upon the details of the lattice. In a circular accelerator, the coefficient is greater than zero since increased momentum implies a longer path. A parameter, the transition gamma γ_t, is defined to characterize this;

$$\frac{\Delta L}{L}=\frac{1}{\gamma_t^2}\frac{\Delta p}{p}. \quad (83)$$

One connects $\Delta p/p$ to $\Delta\beta/\beta=\Delta v/v$ by taking the differential of p and then rewriting Eq. (82);

$$\frac{\Delta p}{p}=\frac{\Delta\left[\left(1-\beta^2\right)^{-1/2}\beta m_o c\right]}{\gamma\beta m_o c}=\frac{\left[\left(1-\beta^2\right)^{-1/2}+\beta^2\left(1-\beta^2\right)^{-3/2}\right]\Delta\beta}{\gamma\beta}=\gamma\frac{\left[1+\dfrac{\beta^2}{1-\beta^2}\right]\Delta\beta}{\gamma\beta}=\gamma^2\frac{\Delta\beta}{\beta}, \quad (84)$$

$$\frac{\Delta\tau}{\tau}=\left[\frac{1}{\gamma_t^2}-\frac{1}{\gamma^2}\right]\frac{\Delta p}{p}=\eta\frac{\Delta p}{p}, \quad (85)$$

where a new parameter, the phase slip factor η, named for its connection with "slip" in phase angle, has been introduced. A kinetic energy T_t corresponds to γ_t where $\eta=0$ and is called the transition energy. This parameter is important as it is a threshold in a change in phase stability illustrated in the middle frame of Fig. 15. For $T<T_t$ and $\eta<0$ an "off-momentum" particle with $\Delta p>0$ has a transit time (revolution period for a complete orbit) of less than that of the synchronous particle due to its greater speed more than compensating for the longer path length it must travel. Above transition ($T>T_t$ and $\eta>0$), the compensation cannot occur, an "off-momentum" particle with $\Delta p>0$ has a longer transit time due to the increased path length it follows. This happens because the speed of a highly relativistic particle no longer increases significantly with momentum, with $\beta\approx 1$. At transition, τ is briefly independent of momentum and all particles are isochronous, with no phase stability. The need to reestablish phase stability during acceleration above transition is addressed by quickly changing the phase of the RF in a phase jump as transition is crossed to assure that above transition, late arriving particles receive a smaller increment of energy so as to take a shorter path on the next orbit to arrive earlier on the next cycle, the opposite to the situation below transition. Likewise, above transition early arriving particles receive more energy to assure a longer path to arrive later the next time around.

Great care is taken to minimize loss of beam at transition. Transition crossing is not a problem at electron synchrotrons since they always operate above γ_t. For most proton synchrotrons, transition crossing is a machine performance issue. Some examples of transition parameters at Fermilab are illustrative; for the T=0.4-8 GeV, R=74.47 m Fermilab Booster, γ_t=5.45 (T=4.17 GeV) and for the T=8-150 GeV, R=528.3 m Fermilab Main Injector, γ_t=20.4 (T=18.2 GeV). For the T=150-980 GeV, R=1000 m superconducting Tevatron, γ_t=18.7 (T=16.6 GeV). Due to its more limited dynamic range of acceleration, the Tevatron always operates above transition.

To digress, in linacs $\eta=-1/\gamma^2$ and is always negative since the path lengths ΔL between accelerating stations do not vary significantly. An isochronous cyclotron always has $\eta=0$ and hence can be said to be always at transition.

Longitudinal Emittance. In longitudinal phase space, $\Delta t \Delta T$ represents the available RF bucket area, the longitudinal acceptance A that must accommodate the beam. For stationary buckets found at injection or maximum energy, with T_s as the energy of the ideal particle and V as the gap voltage,

$$A = \frac{16\beta}{\omega_{RF}} \sqrt{\frac{qVT_s}{2\pi h|\eta|}} \quad (86)$$

Typical values of V are a few MV. If $\Delta\xi$ is the maximum extent of the small oscillations of phase angle (radians) of the beam at injection or at the maximum energy, the longitudinal emittance S that must fit into this bucket area is

$$S = \frac{\pi\beta(\Delta\xi)^2}{\omega_{RF}} \sqrt{\frac{qVT_s}{2\pi h|\eta|}} \quad (87)$$

For accelerating waves, the bucket area shrinks to zero as ξ approaches $\pi/2$ radians so the acceptance must be kept larger than the longitudinal emittance to assure retention of particles. If the particles have too much energy or are too far out of phase, they will be lost. As examples, nominal longitudinal emittances are 0.25, 0.2, and 3 eV s, respectively, for the Fermilab Booster, Main Injector and Tevatron operating in collider mode.

Harmonic Number. As with cyclotrons and synchrocyclotrons, the product $\omega_{rf}\tau_{orbit}=h2\pi$ is the number of RF cycles per particle revolution where h is the harmonic number and τ_{orbit} is the orbit period. It is an integer and generally large. For example, h=84 for the Fermilab Booster, h=588 for the Fermilab Main Injector and h=1113 for the Tevatron in collider mode. The ideal particle will travel around the closed orbit through the center of all magnets with frequency

$$f_{orbit} = \frac{1}{\tau_{orbit}} = \frac{f_{RF}}{h} \quad (88)$$

Establishing and maintaining the closed orbit is an important procedure at all synchrotrons. Often, imperfections and mistunings of one sort or other disrupt the orbit to prevent closure, requiring correction.

Betatron Oscillations and Transverse Emittance. The transverse oscillations about reference orbits, for historical reasons called betatron oscillations, are intrinsic to all circular machines. In a strong-focusing synchrotron they are more complex mathematically than they were for the betatron with the detailed derivations beyond our present purpose. Therefore only summarized results are presented here. The achievement of focusing with multiple quadrupoles in a beamline was discussed earlier. Fig. 15 shows the reference orbit and a commonly used (x,y,s) coordinate scheme. The equations of motion are

$$x'' + K_x(s)x = 0 \quad (89) \text{ and}$$

$$y'' + K_y(s)y = 0 \quad (90)$$

In Eqs. (89) and (90), the primes applied as superscripts denote spatial derivatives with a single prime meaning a first derivative (e.g., $x'=dx/ds$, a "slope") and a double prime denoting a second derivative (e.g., $x''=d^2x/ds^2$). The respective equations for the focusing forces $K_x(s)$ and $K_y(s)$ are

$$K_x(s) = \frac{1}{BR}\frac{\partial B_y(s)}{\partial x} + \frac{1}{R^2}, \quad (91) \text{ and}$$

$$K_y(s) = -\frac{1}{BR}\frac{\partial B_y(s)}{\partial x} \quad (92)$$

These equations, examples of Hill's equation, are analogous to the harmonic oscillator (Kerst-Serber) equations [Eqs. (73) and (80)] found for the betatron and are not unique to synchrotrons. The "centripetal" $(1/R^2)$ term in Eq. (91), shown for completeness, is insignificant for large accelerators, but represents the totality of focusing in a weak-focusing circular accelerator. Some approximations, such as lack of coupling between coordinates x and y and assumptions that the transverse excursions in the orbits are small are used in these equations. Advantage has been taken of Eq. (10) to eliminate all but one partial derivative of magnetic field.

$K_x(s)$ and $K_y(s)$ (i.e., the spring "constants") are functions of location along the s-coordinate. They are constants in the special case of the betatron due to the axial symmetry of that machine. In the synchrotron they are essentially the quadrupole gradients describing the focal properties around the ring through the dependence on s and the deflection with the explicit inclusion of the orbit radius R. Often, they are constants within a given beam element. Periodicity in the accelerator lattices is of help in the solution of these equations since there is a distance C, characteristic of the whole orbit or some defined segment, where

$$K(s+C) = K(s)\ .(93)$$

At many large accelerators with FODO lattices, the *x*- and *y*-dependencies are similar if not identical. With arbitrary constants ε and δ the solution for $x(s)$ is;

$$x(s) = \sqrt{\varepsilon_x \beta_{CS,x}(s)}\cos\left[\psi_x(s)+\delta\right] \text{ and } \frac{d\psi_x(s)}{ds} = \frac{1}{\beta_{CS,x}(s)}\ ,(94)$$

The parameter ε turns out to be the transverse emittance, a property of all particle beams, with the discussion at this point concerning synchrotrons serving as an illustration.

$\beta_{CS,x}(s)$ and $\beta_{CS,y}(s)$ are called the amplitude functions or beta functions; one of set of three Courant-Snyder parameters, and are in units of length as is ε. (The use in this chapter of the subscripts "*CS*" to reduce confusion with other parameters and variables in this discussion is nonstandard.) The maximum value of the amplitude function are exemplified by nominal values of 34 m (horizontal) and 21 m (vertical) in the Fermilab Booster, 58 m in the Fermilab Main Injector, and about 100 m in the Fermilab Tevatron in collider mode. Some number of oscillations in *x* or *y* are found in an orbit. This quantity in, say, the *x*-coordinate ν_x, is, as in the betatron, called the tune in that coordinate. It is generally not an integer and is given by

$$\nu_x = \frac{1}{2\pi}\oint \frac{ds}{\beta_{CS,x}(s)}\ .(95)$$

Tune values are "managed" through the controls to achieve desired properties, for example at injection, transition, or extraction. Examples of nominal tunes in the Fermilab Booster are $\nu_x \approx \nu_y \approx 6.7$ and for the Tevatron in collider mode are $\nu_x \approx \nu_y \approx 19.4$.

Values of the amplitude function are reflective of lengths of the repeat periods and strengths of the lattice elements; these are interpretable as $\pi/2$ times the oscillation's local wavelength. The values ε are small, representative of amplitudes of the transverse oscillations.

The slope, hence the direction (angle) of the particles, can be obtained by evaluating $x'(s)=dx(s)/ds$;

$$x'(s) = -\sqrt{\frac{\varepsilon}{\beta_{CS,x}(s)}}\sin\left[\psi(s)+\delta\right] + \left[\frac{\beta'_{CS,x}(s)}{2}\right]\sqrt{\frac{\varepsilon}{\beta_{CS,x}(s)}}\cos\left[\psi(s)+\delta\right].(96)$$

The pair of coordinates *x* and *x'*, are, like *t* and *T* in connection with Eqs. (86) and (87), the parameters of a phase space. The function $\psi(s)$ is reflective of the focusing strength (i.e., "spring constant") as a function of position in the lattice. As shown in Eqs. (74) and (80), in the betatron these were simply constants times time (equivalent to position) around the circumference. In the synchrotron, $\psi(s)$ has a periodicity reflective of the lattice. At different locations derived from the functional dependencies $\beta_{CS,x}(s)$ and $\beta'_{CS,x}(s)$, *x* and *x'* will cycle through a family of values correlated with designed lattice properties. To do this correctly the remaining Courant-Snyder parameters, inclusive of $\beta_{CS}(s)$, are needed. Since the formalism is the same for the *x* and *y* coordinates, the *x* or *y* subscripts will be omitted in these definitions;

$$\alpha_{CS}(s) = -\frac{\beta'_{CS}(s)}{2}\ ,(97) \text{ and}$$

$$\gamma_{CS} = \frac{1+\alpha_{CS}^2}{\beta_{CS}}\ .(98)$$

The corresponding phase space *xx'* in the synchrotron is bounded by the ellipse

$$\frac{\varepsilon}{\pi} = \gamma_{CS}x^2 + 2\alpha_{CS}xx' + \beta_{CS}x'^2\ .(99)$$

Particle distributions in these transverse coordinates, e.g. $n(x)$, need to be considered and are commonly described by the Gaussian function, here displayed for the *x*-coordinate;

$$n(x)dx = \frac{dx}{\sigma\sqrt{2\pi}}\exp\left[-x^2/2\sigma^2\right],(100)$$

taken as stationary with respect to time at any location *s* (i.e., assuming only small orbit-to-orbit changes). The use of the integral properties of the Gaussian function leads to the following connection of σ with ε:

$$\varepsilon = -\frac{2\pi\sigma^2}{\beta_{CS}} \ln\left[1-F\right], (101)$$

where F is the fraction contained within the ellipse of Eq. (99). Unfortunately various "conventions" in the definition of ε are commonly used that are correlated with the percentage of the beam contained within the ellipse. Examples are $\varepsilon=\sigma^2/\beta$ (15%), $\varepsilon=\pi\sigma^2/\beta$ (39%), $\varepsilon=4\pi\sigma^2/\beta$ (87%), and $\varepsilon=6\pi\sigma^2/\beta$ (95%). The first convention is generally that used at electron accelerators, the second is common at proton machines with the last two sometimes used to characterize "complete" containment of the beam. Fig. 16 shows how the dimensions of the phase space ellipse are connected with the parameters. It also includes an illustration of how the ellipse, of constant area at a given energy defined by the emittance, evolves as a function of location within the FODO structure of the lattice. Two results of great importance are the maximum displacement $x_{\max}$ and maximum angle $x'_{\max}$ that determine the aperture requirements, the admittance of the accelerator;

$$x_{\max} = \sqrt{\frac{\varepsilon\beta_{CS,\max}}{\pi}} \text{ (102) and}$$

$$x'_{\max} = \sqrt{\frac{\varepsilon\gamma_{CS,\max}}{\pi}} . \text{ (103)}$$

In the common situation where a uniform, circular half-aperture of radius a containing no other obstructions is present, the admittance is simply $\pi a^2/\beta_{CS,max}$. During acceleration the emittance shrinks "adiabiatically" but due to relativity the normalized transverse emittance ε_N;

$$\varepsilon_N = \gamma\beta\varepsilon , (104)$$

is invariant. Examples of normalized transverse emittances in the Fermilab Booster, Main Injector, and Tevatron (collider mode) are 8, 30, and 24 π mm milliradian, respectively (95% values). Especially in electron synchrotrons, synchrotron radiation serves to reduce emittance as acceleration occurs, a phenomenon beyond our present scope. The properties of the phase space ellipse are intrinsic to all particle beams, not just those in synchrotrons as exemplified here.

Extraction. Extraction of beam from synchrotrons is accomplished on both a single-turn basis using "kicker" magnets with fast time constants of necessity matched to the orbit period or by resonant extraction where the amplitude function is manipulated to achieve spatially large beam sizes suitable for "splitting" by septa. Electrostatic septa often followed by magnetic elements are used in either method to deflect the extracted beam into the desired channel. At large accelerators, the magnetic elements may be Lambertson dipoles that use the gap field to deflect one beam while a field-free hole in one of the return yokes allows passage of the undeflected beam fraction

Colliding Beams. Special relativity constrains the energy available to investigate fundamental processes in collisions of high energy particles with stationary targets since in such collisions most of the kinetic energy ends up in the relativistic mass m [Eq. (3)]. On the other hand, collisions of particles head-on make essentially all of the kinetic energy available to the reactions being investigated. Thus colliding beam accelerators are needed for key studies of fundamental interactions. To do this the concept of luminosity is of great importance. The interaction rate in collisions of particle beams with solid targets in a fixed (i.e., stationary) target experiment is proportional to the product of the rate of delivery of beam particles times the density of target nuclei in the target multiplied by the reaction probability expressed as the reaction cross section. A good beam current is 1.0 μA ($6.25\text{x}10^{12}$singly-charged particles s^{-1}) and an easily achieved beam spot area might be one cm^2. A solid target has a volume density of target nuclei of $\rho N_A/A$ cm^{-3} where ρ is the density (g cm^{-3}), A is the atomic mass number, and N_A is Avogadro's number ($6.02\text{x}10^{23}$ atoms g-$mole^{-1}$) if cgs units are used (reflective of standard usage). If a 1.0 μA were to interact with a short target of, say, 0.01 m (1.0 cm), the product of this beam current density and target nuclear density is of order 10^{35} $cm^{-2}s^{-1}$. On the other hand, a comparable "beam intensity product" for colliding two one μA beams in a "single pass" arrangement is only about $4\text{x}10^{25}$ $cm^{-2}s^{-1}$ if the beams are of order 1 cm^2 in diameter.

While this difference appears insurmountable at first glance, with colliding beams in synchrotrons advantage is taken of the cyclical return of the beam particles. To do this storage rings are used. The storage rings can be either the same synchrotrons that accelerated the beams or separate rings. Following Desler and Edwards (2004) and using cgs units as is conventional, the average event rate R_{event} (s^{-1}), luminosity L ($cm^{-2}s^{-1}$), and reaction cross section of interest σ_{int} (cm^{-2}) are connected by

$$R_{event} = L\sigma_{\text{int}} \quad (105)$$

With two bunches of beam containing n_1 and n_2 particles, respectively, colliding at frequency f,

$$L = f\frac{n_1 n_2}{4\pi\sigma_x\sigma_y}, \quad (106)$$

where allowance has been made for different values of beam sizes σ_x and σ_y in the x and y coordinates but no allowance has been made here for different lattice properties of the two beams. Choosing $\varepsilon=\pi\sigma^2/\beta$ and denoting by β^* the values of β_{CS}(s) at the interaction point,

$$L = f\frac{n_1 n_2}{4\sqrt{\varepsilon_x\beta^*_{CS,x}\varepsilon_y\beta^*_{CS,y}}}. \quad (107)$$

To maximize luminosity, one thus wants to minimize both the emittance of the beam (an invariant property of the beam independent of lattice position s during storage ring conditions) and the amplitude function. Thus, strong quadrupoles, not surprisingly called low-beta quads, are often used adjacent to collision points to minimize $\beta_{CS,x}$(s) and $\beta_{CS,y}$(s) and thus squeeze the beam into the smallest possible beam spot, while accepting the trade-off of increased angular divergence, at the interaction region. The focusing effects can be dramatic, a value of β^*=0.5 m, compared with $\beta_{CS,\max}$=100 m in the lattice, was achieved before 1993 in the Fermilab Tevatron (Edwards and Syphers 1993). (Ongoing efforts continue to improve luminosity in the Tevatron by reducing both emittances and β^*). If the accelerating synchrotron is also used as the storage ring, these quadrupoles are commonly turned off during acceleration. Evidently, the demands on beam sizes placed on single-pass linear colliders to achieve desired luminosities are severe.

During a given store in a collider, the luminosity will decay with time due to particle collisions, "imperfections", space charge effects, and beam "tails" with eventual need for a new store. Furthermore, even with excellent vacuum systems, the path lengths get to be very long and residual gas scattering can remove particles. The multitude of effects that cause luminosity decay provides many challenges for the accelerator physicists. The integrated luminosity, the time integral of luminosity, is a parameter of accelerator performance of considerable importance since it is tied to the expectation of having some desired number of data events in a given time. For studying rare physics processes, the cross section expressed in units of picobarns (pb) (1.0 pb=$1\text{x}10^{-12}\text{x}10^{-24}\text{cm}^2=1\text{x}10^{-36}\text{cm}^2$) characterizes the reaction probability. The integrated luminosity delivered over some period of time is correspondingly expressed in units of inverse picobarns. As an illustration, at the time of writing, an average value of luminosity during a "good" colliding beam store of protons-antiprotons at the Fermilab Tevatron at T=980 GeV is about $2 \text{ x } 10^{32}$ $\text{cm}^{-2}\text{s}^{-1}$. Thus the achievement of one pb^{-1}, correlated with seeing one event of interest having a one pb cross section, requires, on average, 5000 s (1.4 h) of collisions. Thus to see, on average, one event with one fb (10^{-15} b) cross section would require collection of an average of one fb^{-1} integrated luminosity, corresponding to an operational time of 1400 hours.

Early in the development of colliding beams it was realized that a single ring could be used to collide particles of opposite charge orbiting in opposite directions. This has been achieved for both electrons-positrons and for protons-antiprotons. For the former, low emittance beams of positrons as well as electrons are readily achievable since the positrons can be produced at relatively low energies by the photon-induced pair production process. The situation is different with antiprotons as they must be produced by proton interactions on targets at multi-GeV energies. The antiprotons emerge "divergent" (i.e., with large emittance) and need to be properly packaged into a useful beam for collisions.

Two techniques have emerged that are used individually or collectively usually in a lower energy storage ring. In stochastic cooling, a bunch of particles is treated as a statistical ensemble (hence the name). Statistical deviations from the ideal path are sensed and then adjusted by feedback signals sent across a chord or diameter of the ring to apply a corrective adjustment of some component of the lattice prior to the next arrival of the particular beam bunch. Both CERN and Fermilab have used this to technique to achieve acceptable luminosities for proton-antiproton collisions. In electron cooling, advantage is taken of the large mass difference between the antiprotons and electrons. Since they are both negatively charged, a beam of electrons traveling along with a beam of antiprotons at the same velocity (relativistic parameters β and γ being the same for both) results in the transfer of unwanted transverse momenta of the antiproton to the much lighter electrons analogous to the transfer of heat to a refrigeration medium thermodynamically (hence "cooling" them). Electron cooling has been achieved at several accelerators with perhaps the most dramatic example at Fermilab where T=8 GeV (γ=9.53) antiprotons produced

elsewhere, collected, and cooled stochastically into a beam are successfully further cooled using T=4.36 MeV (γ=9.53) electrons in a unique permanent magnet storage ring. The electrons are supplied using a single-stage pellatron, an ideal accelerator to achieve the required match of electron and antiproton velocities.

Radiation Protection Considerations. The normal accelerator-specific radiation protection considerations discussed previously apply to synchrotrons and storage rings. In particular the parameters that characterize the beams such as the longitudinal emittances and Courant-Snyder parameters are of particular importance especially if the acceptances are close to the minimal values, as commonly occurs. Also, in the "tails" of the distributions, the description of beam by Gaussian functions may be invalid since far into these tails, small fabrication imperfections and alignment errors may render the Gaussian picture an incomplete one. As with other circular accelerators, extracted beams represent the need to consider the single pulse accident scenario. Within the accelerator during acceleration or in storage ring mode, a careful, conservative assessment of plausible accident conditions may be useful since analysis of the lattice and associated beam properties could render the loss of the entire beam at a single point non-plausible. Furthermore, with a circulating beam, the plausibility of point losses of the entire contents of the machine needs to be assessed.

Single-turn and resonant extraction methods pose challenges. Single-turn extraction occurs over time periods too short to accommodate the time required to implement some corrective measures otherwise useful for adjusting for "errors". Resonant extraction can create large beam sizes resulting in "lossy" conditions if missteered. The special properties of long term storage of particles in colliders and synchrotron radiation sources merit attention. Duty factor considerations are important at synchrotrons. Collaboration of radiation protection professionals with accelerator physicists can be of significant value in understanding these matters.

FUTURE POSSIBILITIES

The present techniques discussed above in common use that achieve successful acceleration of particles rely on methods and concepts that originated decades ago. Groups of particles are guided and accelerated by the application of static and dynamic electromagnetic fields. While the application of the technology of superconductivity represents a major advance in achieving these objectives, the fundamental methods are unaltered in that macroscopic, not microscopic, electromagnetic fields are used. While the application of special relativity is crucial, there are essentially no connections with the quantum world.

As stated before, due to phase velocity considerations electromagnetic waves do not accelerate particles directly in a vacuum. Indeed, in view of Eq. (43), the direction of propagation of the energy of electromagnetic waves in free space is orthogonal to both $\boldsymbol{E}$ and $\boldsymbol{B}$. Also, while it would be nice to use photons (i.e., "light"), readily available with intense energy densities in the form of lasers, to accelerate particles an individual photon cannot transfer all of its energy to a charged particle due to the need to conserve momentum and energy.

However, it is possible to use photons collectively to accomplish acceleration. One can, in principal, use plasma waves generated by lasers to, in effect, "drag" charged particles along by the electromagnetic fields in their "wake" much as occurs with water waves behind a boat. Such plasma waves should have electric field strengths of order 10-100 GV m^{-1} compared to the limitation of RF fields to 10-50 MV m^{-1}. Difficulties encountered in the path of exploiting this technique lie in the inability to maintain the required laser intensity over the distances needed to reach desired energies, huge energy spreads in the accelerated particle spectrum, and slippage between the velocity of relativistic particles (β=1) and that of the wake (β<1). An encouraging recent development is the successful acceleration of an electron beam to 1.0 GeV in a 0.033 m long gas-filled capillary discharge waveguide by Leemans et al. (2006) at the Lawrence Berkeley National Laboratory (LBNL). The energy spread at one GeV was approximately 100 MeV FWHM, still very large but promising for future work. There are other critical technical challenges that remain resolved such as difficulties in scaling the technique up to high energies, the ability to accelerate large beam currents, and the requirement to achieve acceptable (i.e., "small") emittances. Other methods utilizing lasers and plasmas are also being pursued.

At the quantum level, it should be realized that interatomic electromagnetic and nuclear forces are far stronger than those presently obtainable macroscopically. It is recognized that the ability to exploit the high electromagnetic fields available microscopically could provide accelerators that would not require huge, costly installations. In a development along these lines, small silicon crystals (0.039 m long by 0.003 m high by 0.009 m wide) have used to extract 900 GeV protons from the Tevatron in a "demonstration" experiment of channeling by the crystal planes. A 0.64 milliradian deflection of the beam was achieved by mechanically bending the crystal lattice (Carrigan et al. 2002). While this bend seems small, to accomplish this in a distance of only 0.039 m with a

uniform static electric field would require $\boldsymbol{E}$=14.8 GV m^{-1} [Eq. (17)] or a uniform static magnetic field of $\boldsymbol{B}$=49.3 T [Eq. (20)]. Both values are well beyond present capabilities in the macroscopic realm.

The duty of the accelerator health physicist is to maintain familiarity with these intriguing developments with an awareness of other safety considerations that might be present.

ACKNOWLEDGMENTS

It is hoped that this discussion has aroused curiosity in the reader beyond the limited discussion provided here. The author gratefully acknowledges the critical comments provided by Drs. Michael Syphers (Fermilab), Kamran Vaziri (Fermilab), and Alexander Elwyn (Fermilab, retired) who kindly reviewed the manuscript. The author appreciates the support of Mr. William Griffing (Fermilab) in participating in this effort. Most of all, I thank my wife Claudia for her encouragement and her patience with a considerable amount of work done at home.

REFERENCES

Bryant PJ, Johnsen K. The principles of circular accelerators and storage rings. New York, NY: Cambridge University Press; 1993.

Carey DC. The optics of charged particle beams. New York, NY: Harwood Academic Publishers; 1987.

Carrigan RA Jr, Chen D, Jackson G, Mokhov N, Murphy CT, Baker S, Bogacz A, Cline D, Ramachandran S, Rhodes J, Rosenzweig J, Asseev A, Biryukov V, Taratin A, Ellison JA, Khanzadeev A, Prokofieva T, Samsonov V, Solodov G, Newberger B, Tsyganov E, Shih H-J, Gabella W, Cox B, Golovatyuk V, McManus A. Beam extraction studies at 900 GeV using a channeling crystal. Phys Rev Special Topics-Accelerators and Beams 5: 043501-1 to 043501-24; 2002. Early results were reported by Murphy CT et al. First results from bent crystal extraction at the Fermilab Tevatron. Nucl Instrum and Meth B199:231-238; 1996.

Desler K, Edwards DA. Accelerator physics of colliders. Phys Lett B592:235-238; 2004.

Edwards DA, Syphers MJ. An introduction to the physics of high energy accelerators. New York, NY: John Wiley and Sons, Inc.; 1993.

FMI Website. Fermi National Accelerator Laboratory Accelerator Division Main Injector Department Website [online]. Available at http://www-fmi.fnal.gov/. Accessed 25 June 2007.

Jackson JD. Classical electrodynamics. 3rd ed. New York, NY: John Wiley and Sons, Inc.; 1999.

Jahnke E, Emde F. Tables of functions with formulae and curves. 4th ed. New York, NY: Dover; 1945.

Lee SY. Accelerator physics. Singapore: World Scientific; 2004.

Leemans WP, Nagler B, Gonsalves AJ, Toth C, Nakamura K, Geddes CGR, Esarey E, Schroeder CB, Hooker SM. Nature Phys 2:696-699; 2006[serial online]. Available at http://www.nature.com/nphys/archive/index.html. Accessed 25 June 2007.

Livingood JJ. Principles of cyclic particle accelerators. New York, NY: D Van Nostrand; 1961.

Wangler T. RF linear accelerators. New York, NY: John Wiley and Sons, Inc.; 1998.

Wiedemann H. Classical mechanics and electro-magnetic theory. Course presented at U. S. Particle Accelerator School at Williamsburg, VA, January 2004 [online]. Available at : http://uspas.fnal.gov/CMandEM.pdf. Accessed 25 June 2007.

Wilson E. An introduction to particle accelerators. New York, NY: Oxford; 2001.

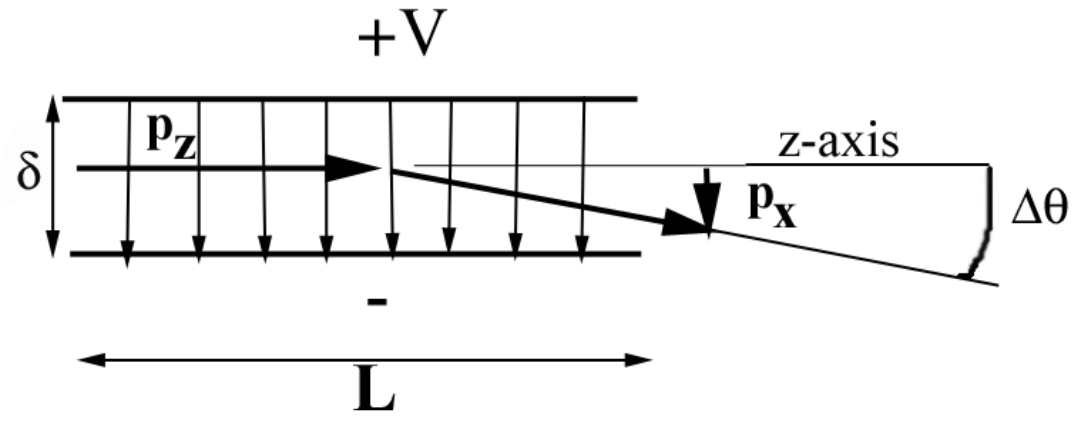

Fig. 1 Parallel plate electrostatic deflector comprised of two parallel plates of length L and separation distance δ biased at voltage V. The vertical arrows denote the resultant electric field oriented along the x-axis. Particles of positive charge q enter from the left along the z-axis with momentum $p=p_z$ and exit with an additional component along the x-axis p_x. The angular deflection measured from the center of the deflector is $\Delta\theta$.

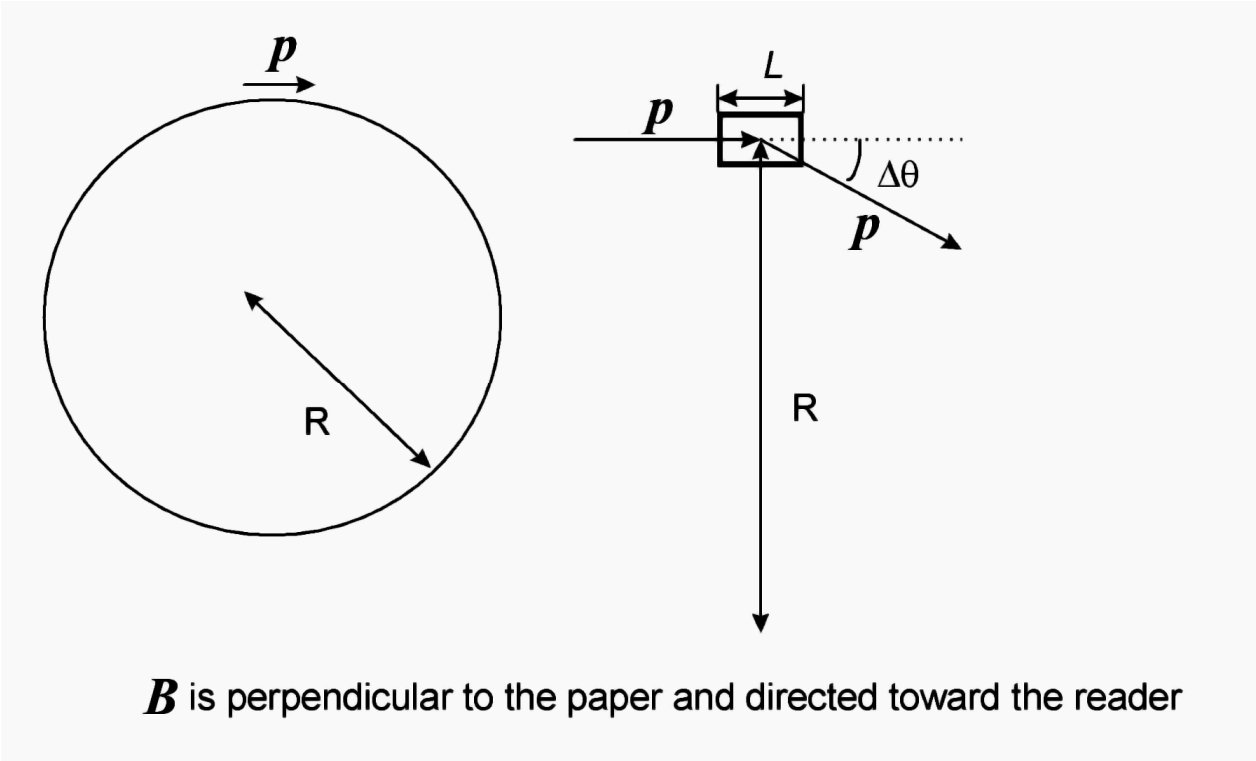

Fig. 2 A particle of positive charge q having momentum $\boldsymbol{p}$ follows a circular path when directed perpendicular to a static, uniform magnetic field $\boldsymbol{B}$. The left frame illustrates this for a complete circle. In the right frame, a particle of momentum $\boldsymbol{p}$ enters a magnet of length L that has a field integral value of BL. For this example, $L<<R$ and the particle experiences a small angular deflection $\Delta\theta$. The angular deflection is exaggerated for clarity.

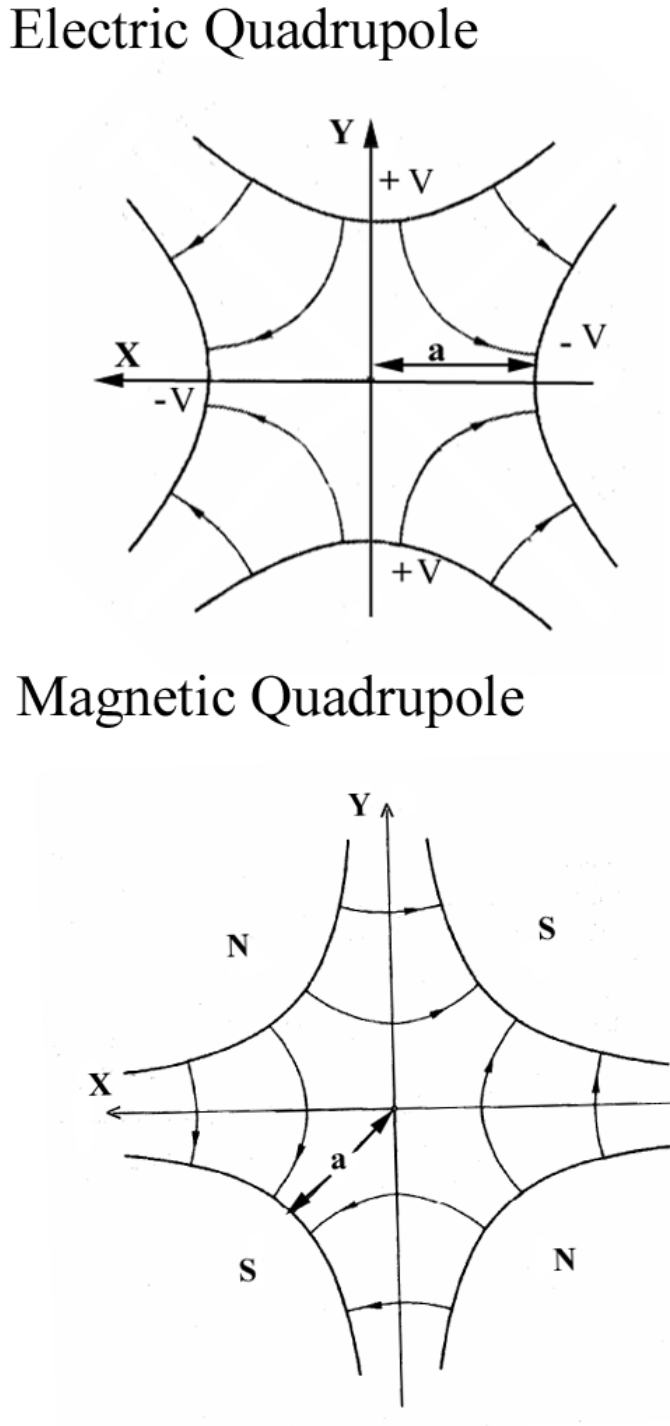

Fig. 3 Cross section of typical electric (top) and magnetic (bottom) quadrupoles. The pole pieces are of polarities configured as shown, denoted "+V" and "-V" for the electric version and “N” and “S” for the magnetic version. A Cartesian coordinate system is shown where *x* and *y* denote transverse coordinates while *z* is along the desired beam trajectory, the optic axis of the beam optical system. In this figure, the beam enters the quadrupoles into the paper along the positive *z*-axis. The curves with arrows are the respective electric and magnetic field lines. The field orientations shown achieve focusing for positively charged particles in the *yz* plane.

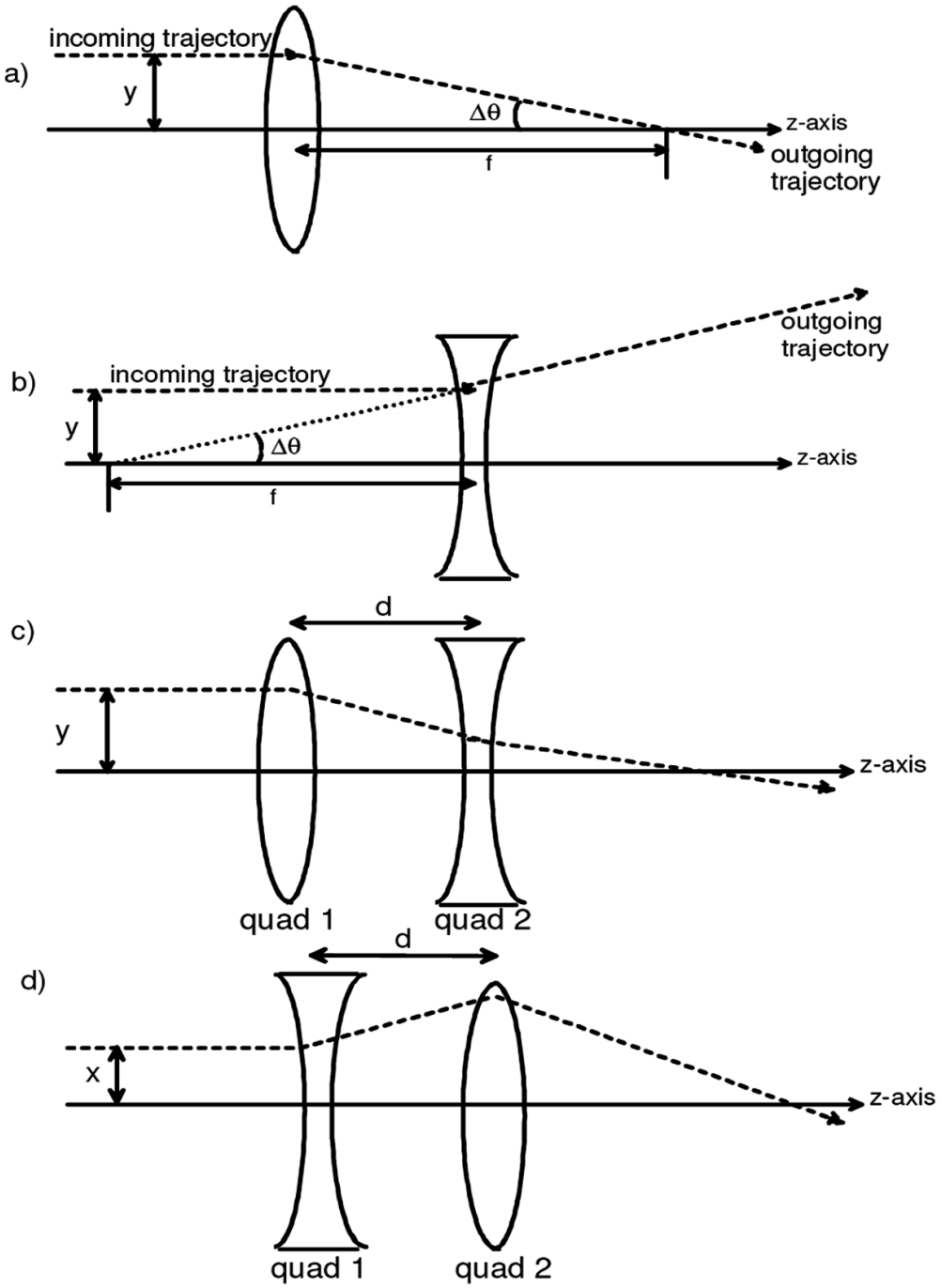

Fig. 4 Configurations of quadrupole lenses are shown with the symbolism explained in the text: a) Representation of focusing in the *yz* plane of a beam trajectory incident from the left parallel to the *z*-axis. A real image is formed at the focal length *f* from the lens. b) Representation of defocusing in the *yz* plane. The parallel beam is deflected so that it appears to emerge from a point a distance *f* before the lens, thus, forming a virtual image. c) Representation of a particle trajectory in the *yz* plane of a quadrupole doublet. The particle enters a quadrupole doublet parallel to the *z*-axis from the left. First a focusing quadrupole (quad 1) is encountered and then a defocusing quadrupole (quad 2) follows. d) Representation of a particle trajectory in the *xz* plane of the same doublet. The particle enters the doublet parallel to the *z*-axis. In *xz* plane the defocusing quadrupole is encountered first.

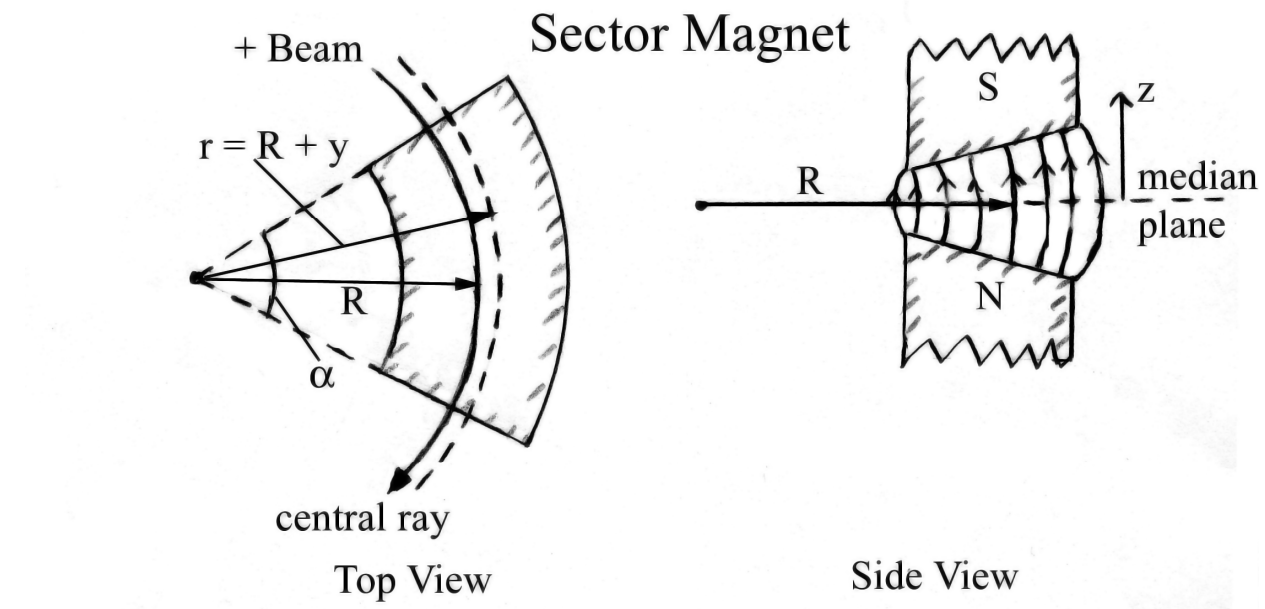

Fig. 5 Top and side views of a sector magnet of non-uniform magnetic field. The top view shows the central ray at radius $r=R$ followed by a beam of positively-charged particles along with a path taken at a slightly larger radius $r=R+y$. The side view shows the radially non-uniform magnetic fields that achieve the deflection shown.

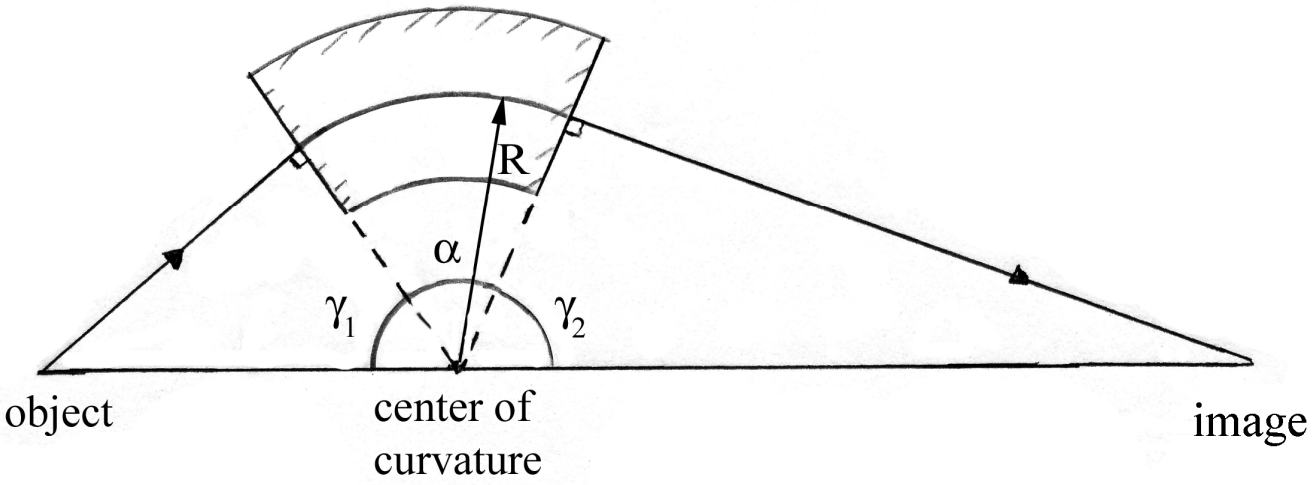

Fig. 6 Formation of an image by a uniform field sector bending magnet showing the central ray and the alignment of the object, center of curvature points, and image points in accordance with Barber's Rule.

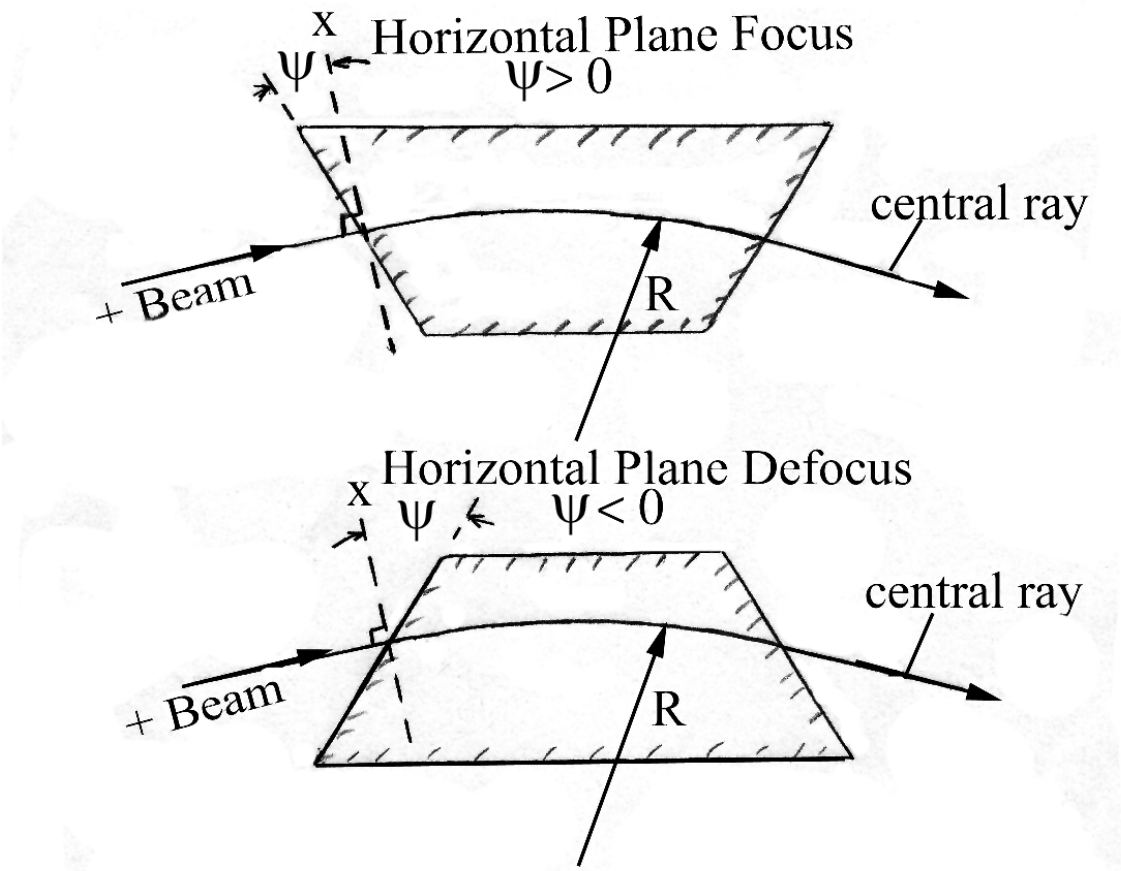

Fig. 7 Plan views of uniform field "wedge" magnets that are set up to focus (upper frame) and defocus (lower frame) in the horizontal plane. In each the central ray is a circle of radius *R* and is shown for positively charged particles.

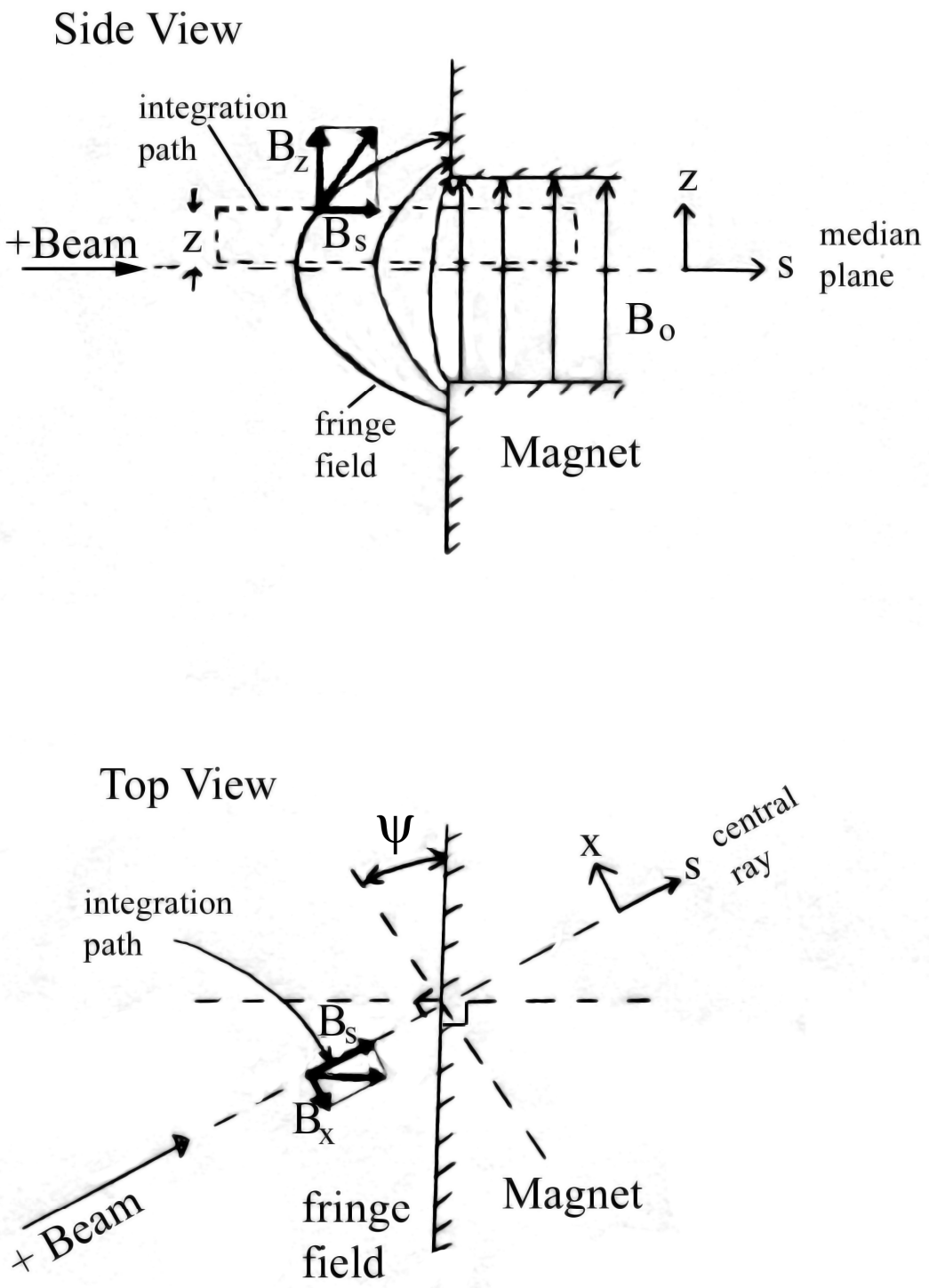

Fig. 8 Side (top) and plan (bottom) views of a uniform field "wedge" magnet set up to focus incoming positively charged beam particles in the vertical (i.e., non-bending) plane. The coordinate system discussed in the text is defined along with components of the magnetic field strength vector and the integration path used in the application of Eq. (10).

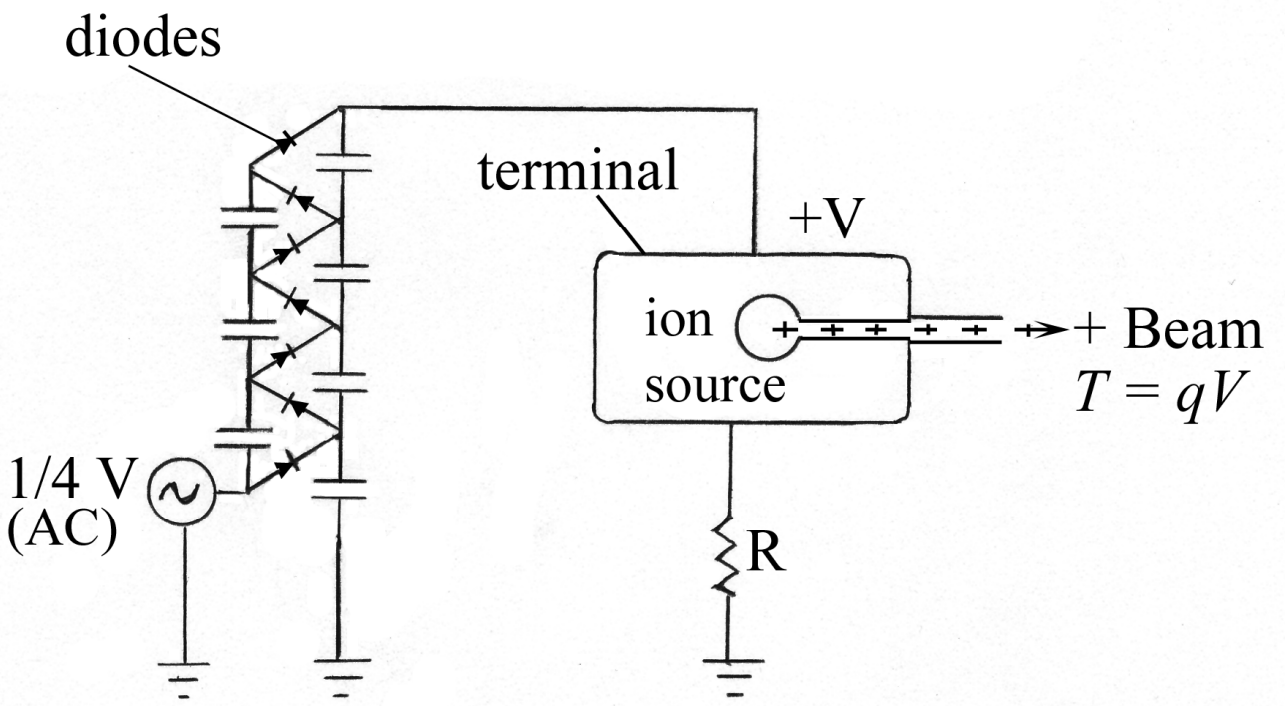

Fig. 9 Schematic diagram of a Cockcroft-Walton electrostatic accelerator with 4 stages. The alternating voltage ¼ *V* (rms) is converted to a rectified voltage *V* at the terminal containing the charged particle source by means of the "ladder" rectifier circuit shown. The electrical resistance *R* between the terminal and ground is essentially infinite. Particles of positive charge *q* produced by the source emerge with kinetic energy $T=qV$.

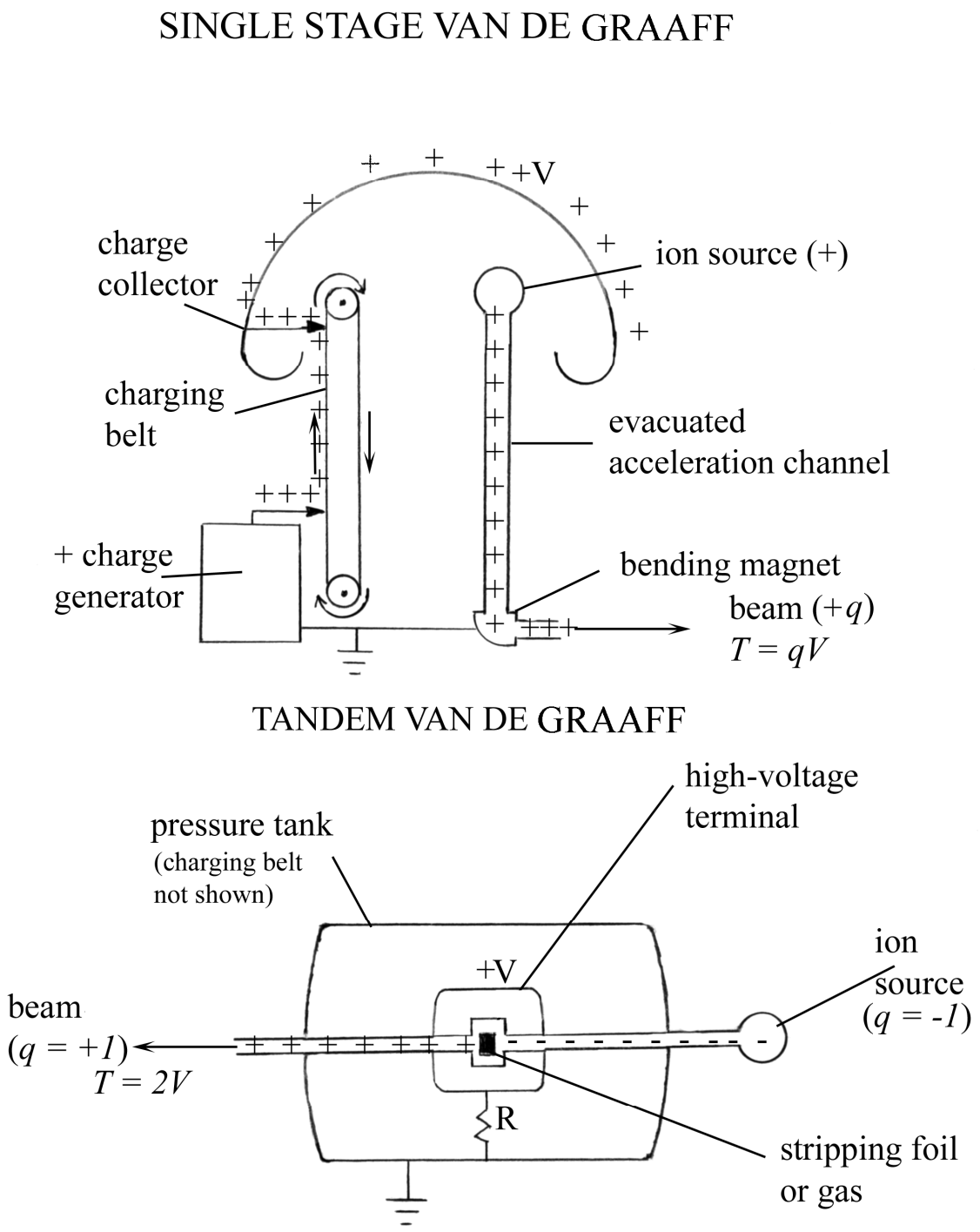

Fig. 10 Schematic diagram of single stage (top frame) and tandem (bottom frame) Van de Graaff accelerators. The pressure tank and essentially infinite resistance between terminal and ground is not shown for the single stage machine. The charging belt assembly is located inside the pressure tank in both versions but is not shown for the tandem.

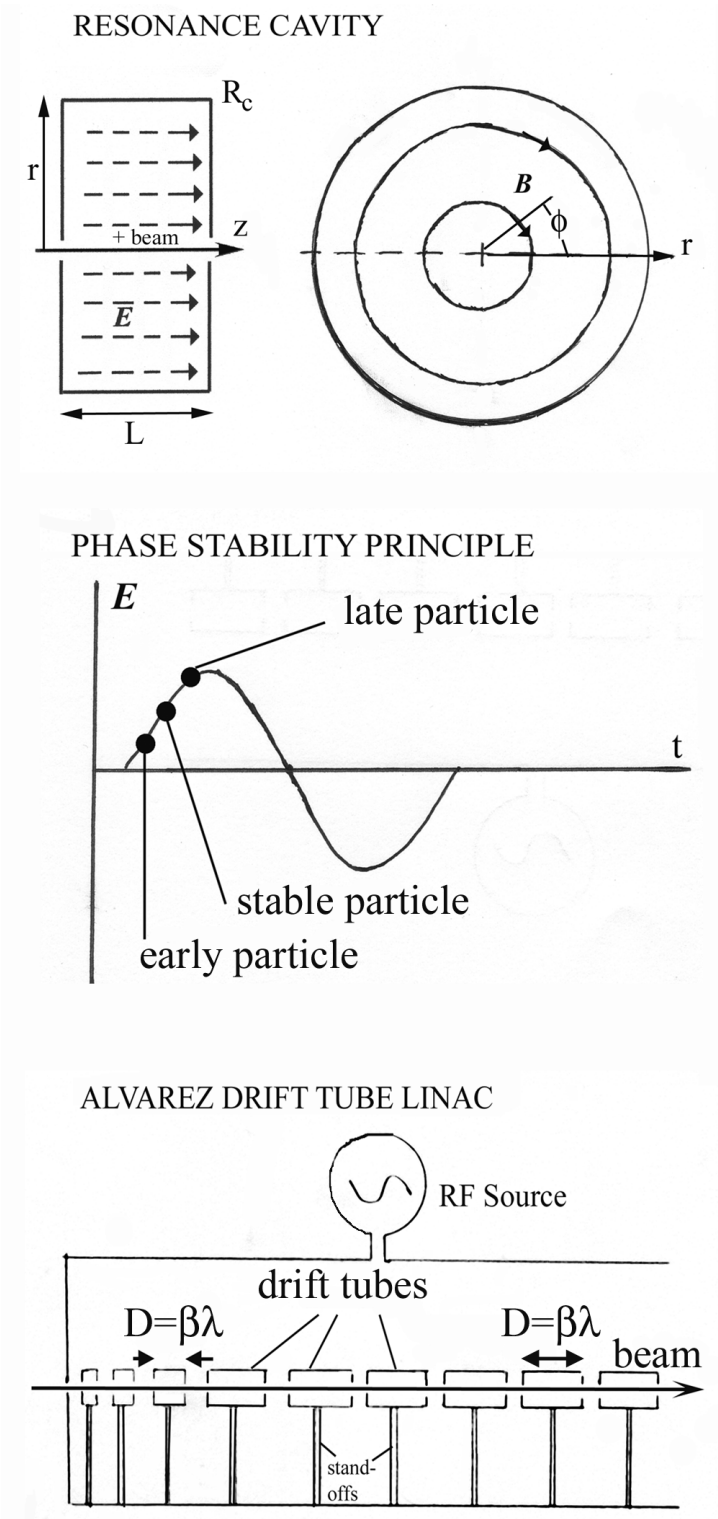

Fig. 11 Features of resonant acceleration. The top frame displays a conductive cylindrical resonance "pillbox" cavity of radius R_c and length L excited by a longitudinal sinusoidal electric field of strength $\boldsymbol{E}(t)$. The left view is in the zr plane with the electric field lines shown during acceleration of positive particles. The right view shows a "beam's eye" view down the cavity with magnetic field lines shown along with the definition of the azimuthal angle ϕ. The middle frame shows the principle of phase stability where the applied sinusoidal electric field $\boldsymbol{E}(t)$ is shown as a function of arrival time t for "early", "stable", and "late" particles. The bottom frame illustrates an Alvarez drift tube linac including the RF source, the drift tube tank, the drift tubes and their standoffs.

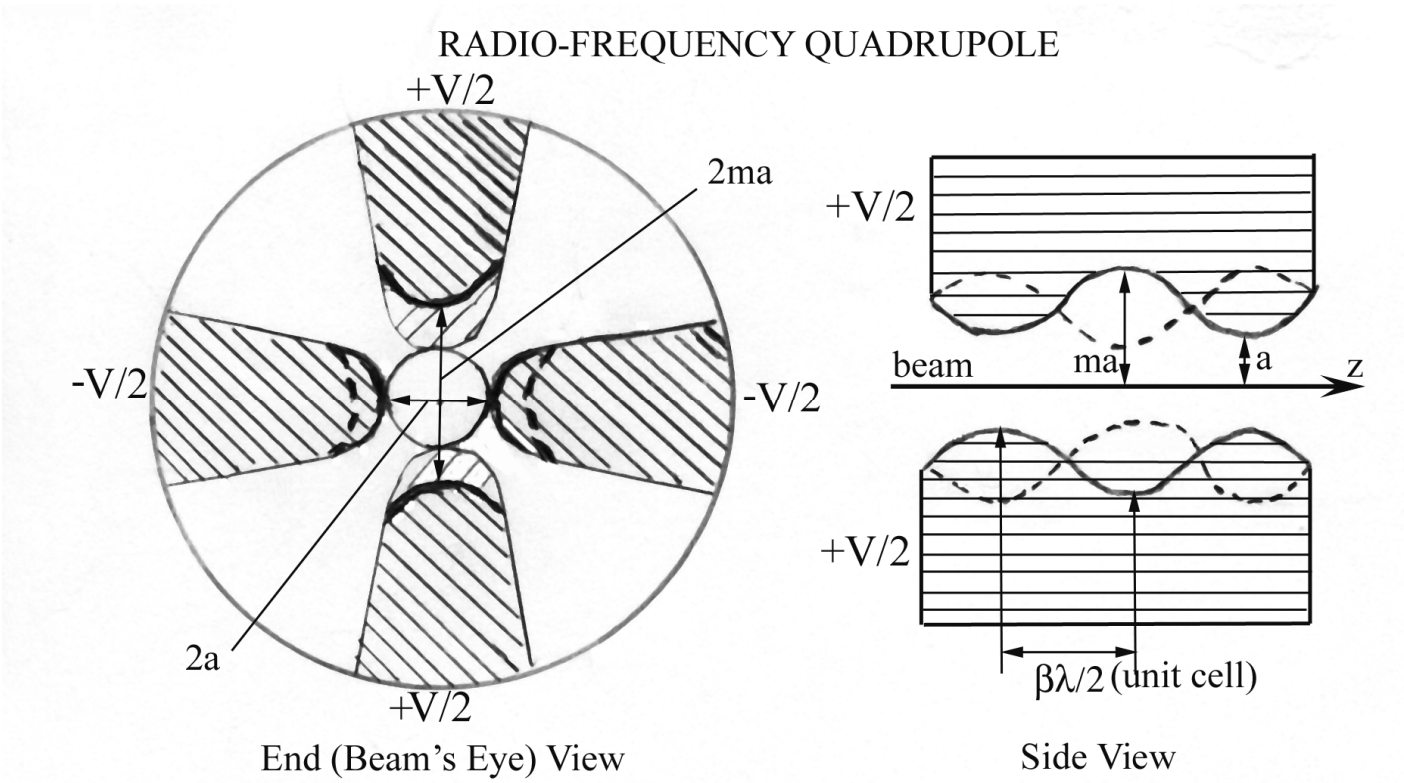

Fig. 12 The left side is a transverse (beam's eye) view of a radio-frequency quadrupole (RFQ) defining the transverse coordinates *x* and *y*. The cross-hatched areas represent the "vanes" excited to generate the RF quadrupole field that simultaneously focuses and accelerates the beam particles. The right side defines the unit cell length and the modulation factor *m* along with the longitudinal *z*-axis. The cross-hatched area represents one pair of cells such as the *yz* pair while the profile indicated by the dashed modulation curve represents the other pair, here as the *xz* pair.

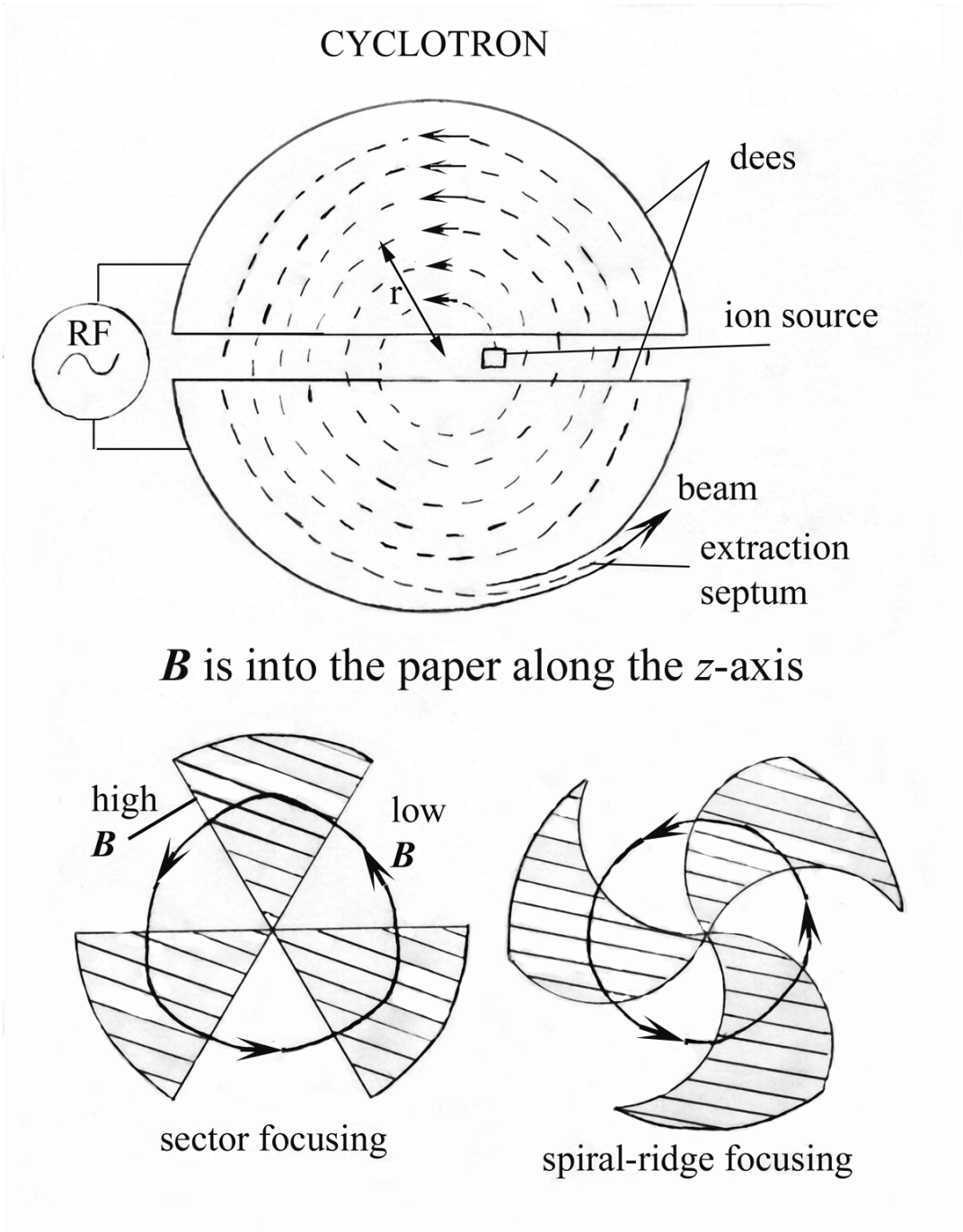

Fig. 13 Schematic drawing of a cyclotron. The top frame is a plan view showing the dees, orbits, RF source, and extraction septum for positive particles being accelerated with the magnetic field directed into the paper. The bottom frame shows illustrations of sector and spiral-ridge focusing arrangements for the same magnetic field configuration.

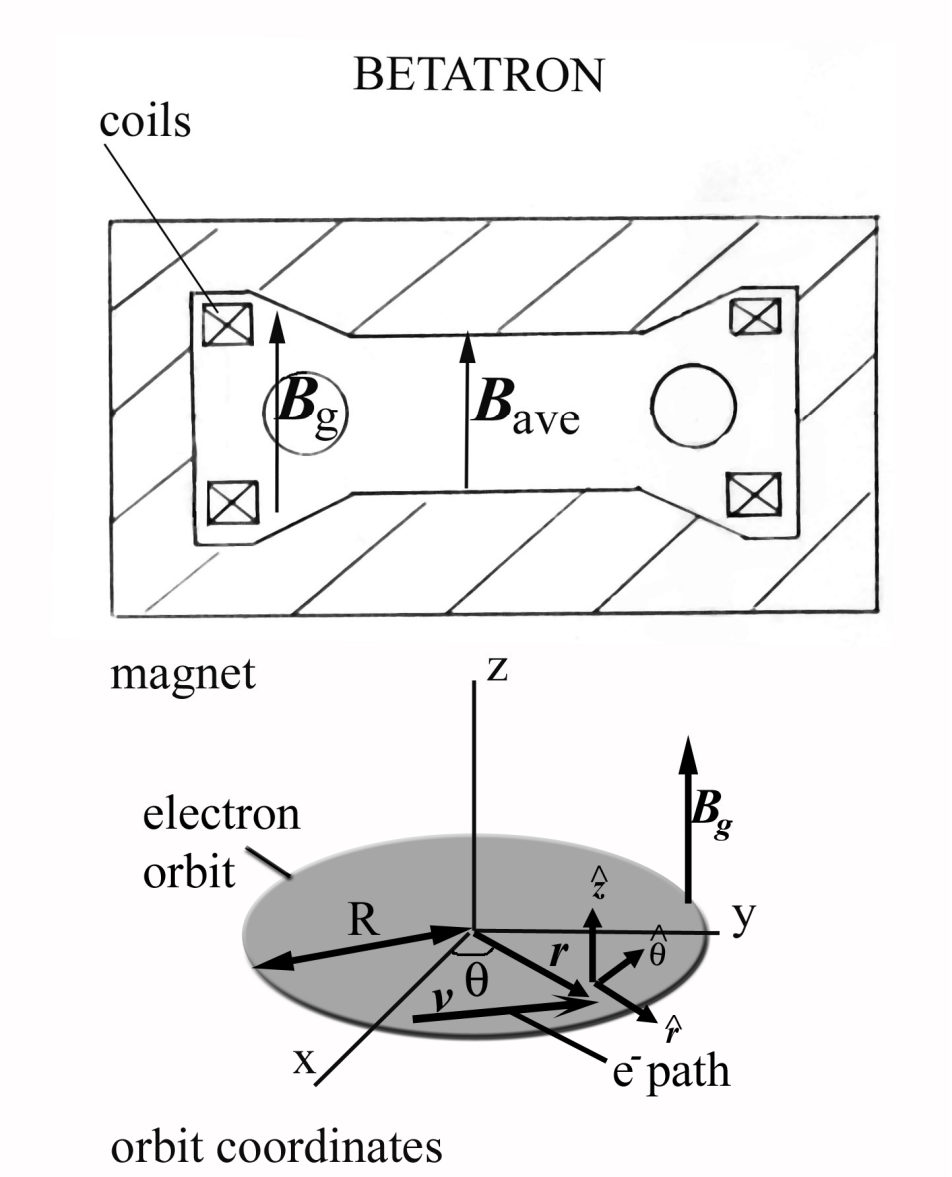

Fig. 14 View of a betatron set up to accelerate negatively charged particles, usually electrons. The top frame is a side view of the magnet with its field configuration set up to achieve the guide field $B_g=1/2B_{ave}$ at orbit radius R. The bottom frame shows the cylindrical coordinates that describe the motion near the orbit plane indicated by the disk. The unit vectors corresponding to the coordinates (r,θ,z) are defined.

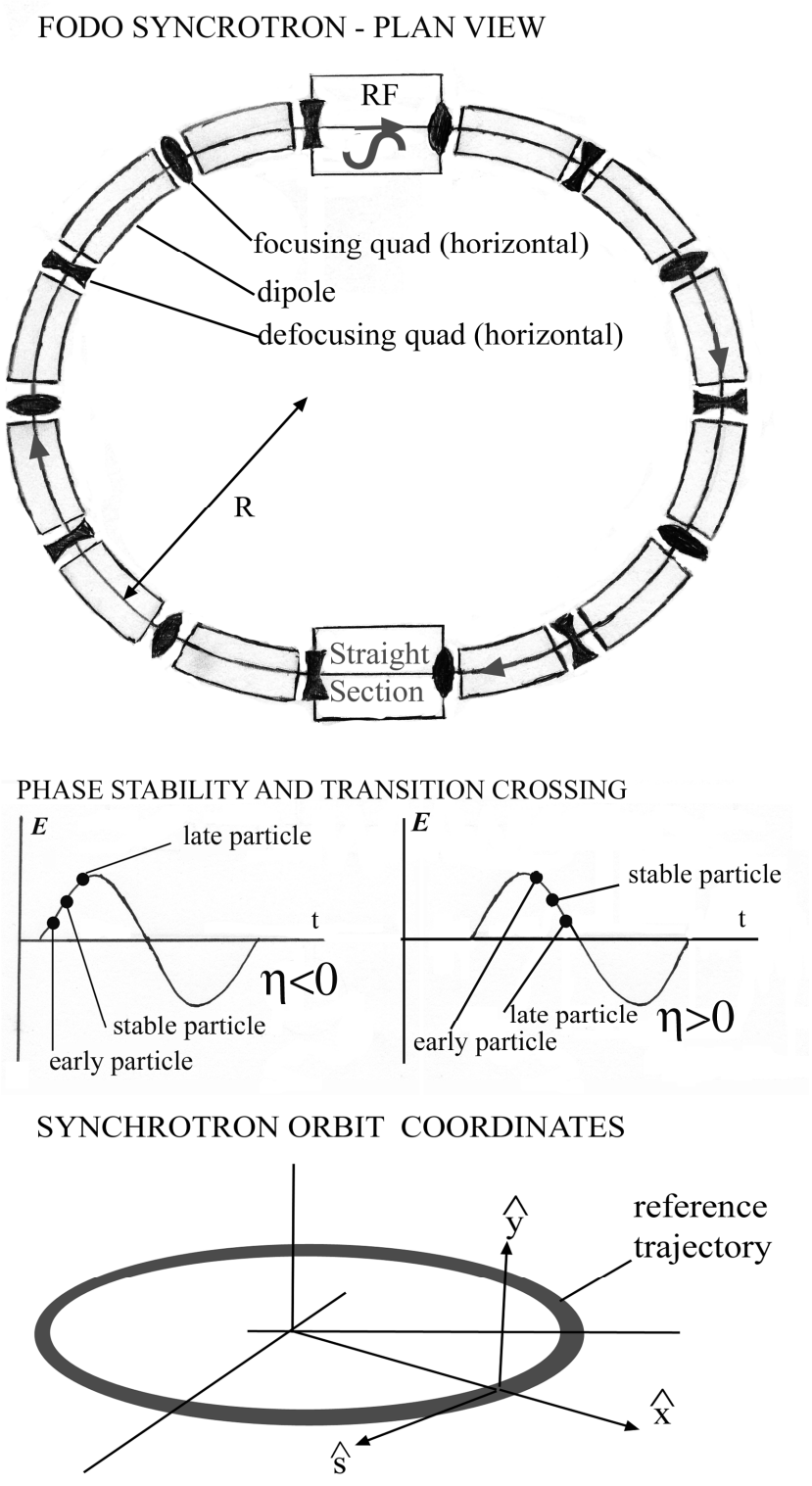

Fig. 15 The top frame is a plan view sketch of a FODO synchrotron showing the bending dipoles, quadrupole magnets that focus (defocus) and defocus (focus) in the horizontal (vertical) plane along with two examples of straight sections, one with RF cavities and the other assigned to other uses (e.g., injection, extraction, experiments). The middle frame shows phase stability conditions below (η<0) and above (η>0) transition. The bottom frame shows the unit vectors that describe the coordinates applied to the orbital path (x,y,s) where the s-axis measures positions along the path of the ideal particle.

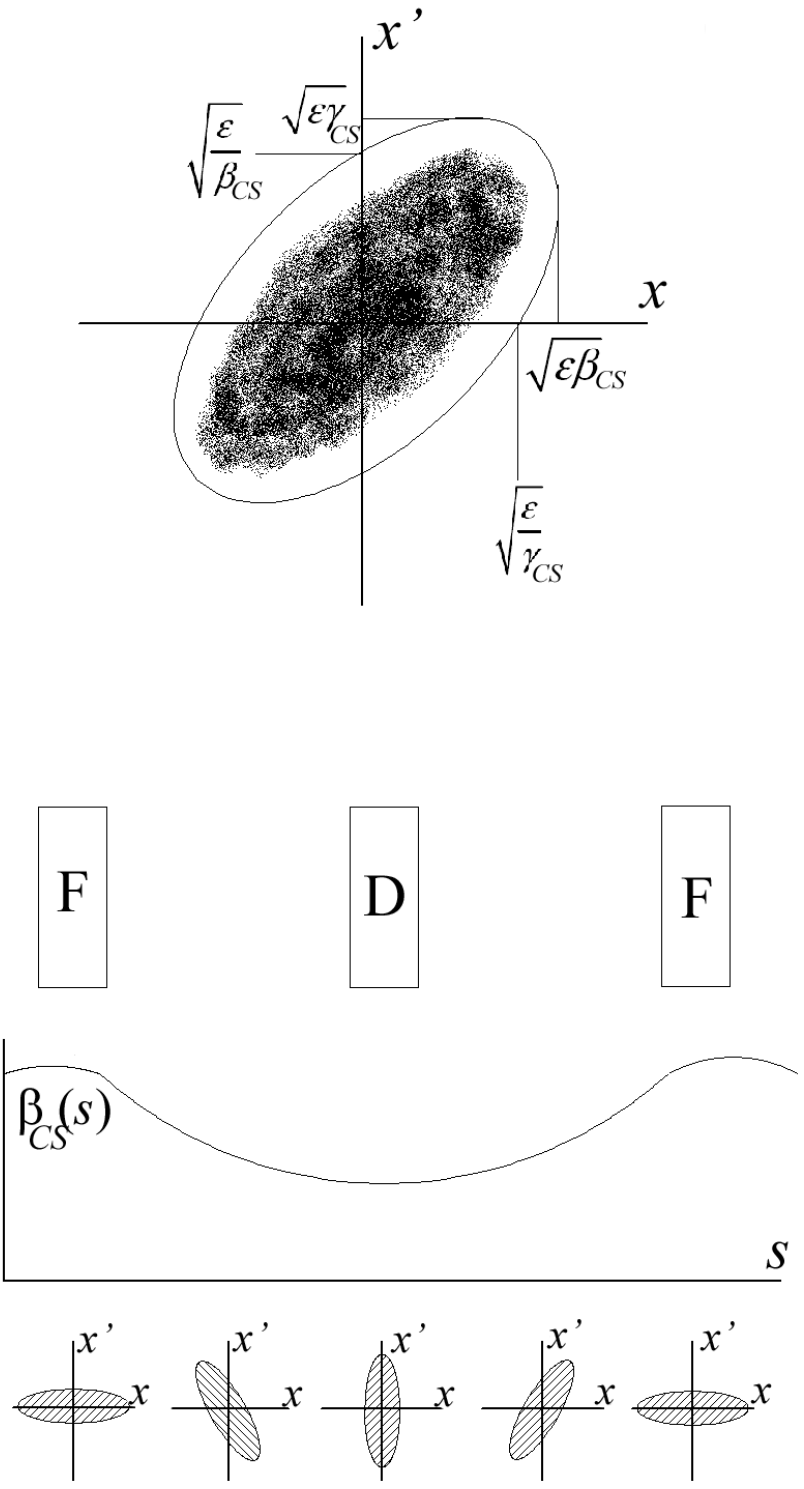

Fig. 16 Illustration of the transverse phase space behavior of a particle beam having Courant-Snyder parameters β_{CS} and γ_{CS}, here for the *x*-coordinate. The top frame shows a typical phase *xx'* phase space ellipse. The "dots" represent of individual beam particles. The bottom frame shows the evolution of the ellipse and the amplitude function $\beta_{CS}(s)$ on position *s* in the lattice. "F" and "D" are focusing and defocusing quadrupoles in the *xs* plane.